Modelling the processes driving Trichodesmium sp. spatial distribution and biogeochemical impact in the tropical Pacific Ocean

Cyril Dutheil[1,2], Olivier Aumont[2], Thomas Gorguès[3], Anne Lorrain[4], Sophie Bonnet[5], Martine Rodier[6], Cécile Dupouy[5], Takuhei Shiozaki[7], Christophe Menkes[1,2]

[1]Centre IRD, Nouméa, New Caledonia

[2]LOCEAN Laboratory, IPSL, Sorbonne Universités (UPMC, Univ Paris 06)-CNRS-IRD-MNHN, Paris, France

[3]Laboratoire d'Océanographie Physique et Spatiale (LOPS), *Univ. Brest-CNRS-Ifremer-IRD, Plouzané, France*

[4]LEMAR, UMR 6539, *UBO-CNRS-Ifremer-IRD, IUEM, Plouzané, France*

[5]Aix Marseille Université, CNRS/INSU, Université de Toulon, IRD, Mediterranean Institute of Oceanography (MIO) UM 110, 13288, Marseille, France

[6]Environnement Insulaire Océanien (EIO), *UMR 241(Univ. de Polynésie Française, IRD, ILM, IFREMER), Tahiti, French Polynesia*

[7]Research and Development Center for Global Change, *Japan Agency for Marine-Earth Science and Technology, Yokosuka, Japan*

Correspondence to: Cyril Dutheil (cyril.dutheil@ird.fr)

Abstract. Dinitrogen fixation is now recognized as one of the major sources of bio-available nitrogen in the ocean. Thus, nitrogen fixation sustains a significant part of the global primary production by providing an input of the most common limiting nutrient for phytoplankton growth. Evidences of the Western Tropical South Pacific being a hotspot of nitrogen fixation, and a data coverage complemented by OUTPACE, lead us to develop an explicit nitrogen fixation compartment based on the *Trichodesmium* physiology (the most studied nitrogen fixer) within a 3D coupled dynamical-biogeochemical model (ROMS-PISCES). We performed a first 20-year tropical Pacific simulation that is able to reproduce the main physical (e.g Sea Surface Temperature) and biogeochemical conditions (nutrients, and chlorophyll concentrations as well as dinitrogen fixation). This simulation showed a possible *Trichodesmium* regional distribution that extends from 150°E to 120°W in the south tropical Pacific, and from 120°E to 140°W in the north tropical Pacific. The local simulated maximums were around islands (Hawaii, Fiji, Samoa, New Caledonia, Vanuatu). We assessed that 15% of the total primary production may be due to *Trichodesmium* in the Low Nutrient, Low Chlorophyll regions (LNLC). We also argue that implicit parameterization of N_2 fixation (often used in biogeochemical models) leads to underestimate nitrogen fixation rates by about 25% in LNLC regions compared to our explicit formulation. Finally, we showed that iron fluxes from island sediments control the spatial distribution and the abundance of *Trichodesmium* in the western tropical south Pacific. Noteworthy, this last result does not take into account the iron supply from rivers and

36 hydrothermal sources, which may well be of importance in a region known for its strong precipitation rates and volcanic

37 activity.

38

1. Introduction

40

41 Nitrogen is known to be the most common limiting nutrient for phytoplankton growth in the modern world ocean

42 (Moore et al., 2013), especially in the Low Nutrient, Low Chlorophyll (LNLC) ecosystems (Arrigo, 2005; Gruber,

43 2005). Characterizing the processes governing nitrogen sources and sinks to and from the ocean is therefore central to

44 understanding oceanic production, organic matter export and food web structure. Atmospheric dinitrogen (N_2) dissolved

45 in seawater is by far the dominant form of N present in the ocean, i.e. the $N_2:NO_3^-$ ratio typically exceeds 100 in surface

46 waters. However, most phytoplankton species cannot assimilate N_2, and grow using reactive forms of nitrogen such as

47 nitrate, ammonium and dissolved organic compounds. Some planktonic prokaryotic microorganisms, called

48 "diazotrophs" use an enzyme, the nitrogenase, to fix N_2 and convert it into ammonia (NH_3) and ultimately ammonium

49 (NH_4^+). At the global scale, they provide the major external source of reactive nitrogen to the ocean (Gruber, 2008), and

50 support up to 50% of new production in tropical and subtropical (LNLC) regions (Bonnet et al., 2009; Capone, 1997;

51 Deutsch et al., 2007; Karl et al., 1997; Moutin et al., 2008; Raimbault and Garcia, 2008). These organisms are

52 physiologically and taxonomically diverse including cyanobacteria, bacteria, archaea (Zehr and Bombar, 2015; Delmont

53 et al., 2017)(Delmont et al., 2017; Zehr and Bombar, 2015).

54 Autotrophic diazotrophs have been far more intensively studied than heterotrophic diazotrophs, whose contribution to

55 global N_2 fixation remains unclear (Turk-Kubo et al., 2014; Bombar et al., 2016; Moisander et al., 2017)(Bombar et al.,

56 2016; Moisander et al., 2017; Turk-Kubo et al., 2014). Autotrophic diazotrophs have been characterized both in the field

57 and through laboratory experiments and their physiology is consequently better (Bergman et al., 2013; Küpper et al.,

58 2008; Mulholland et al., 2001; Mulholland and Capone, 2000; Ohki et al., 1992; Ramamurthy and Krishnamurthy,

59 1967; Rubin et al., 2011). Cyanobacterial (autotrophic) diazotrophs are composed of 3 main groups: 1) the filamentous

60 diazotrophs including the colonial, non-heterocyst-forming *Trichodesmium*, 2) the heterocyst-forming symbionts

61 associated with diatoms (DDAs), and 3) the unicellular cyanobacterial diazotrophs (UCYN, phylogeneticaly divided

62 into three groups :, UCYN-A, B, and C). It has been established that autotrophic diazotrophs growth rates are typically

63 one order of magnitude lower than those of non-diazotrophs (Breitbarth et al., 2008; Falcón et al., 2005; Goebel et al.,

64 2008; LaRoche and Breitbarth, 2005). This can be related to the high energetic demand (Postgate, 1982) required to

65 convert N_2 to NH_3 as compared to that necessary to assimilate nitrate or ammonia. This low growth rate (compared to

66 other phytoplankton species) mainly constrains their ecological niches to nitrate-poor regions, where they can be

67 competitive. Moreover, their geographical distribution is constrained by nutrient availability in the photic layer (mainly

68 iron and phosphate) (Berman-Frank, 2001; Bonnet et al., 2009; Mills et al., 2004; Moutin et al., 2005, 2008; Rubin et

69 al., 2011; Rueter, 1988) and temperature (Staal et al., 2003). Trichodesmium sp. are present only in water where

70 temperature is above 20°C (Capone, 1997; LaRoche and Breitbarth, 2005; Montoya et al., 2004), while some UCYN

71 can be found in colder and deeper waters (Bonnet et al., 2015a; Church et al., 2005; Moisander et al., 2010)

72 The spatial distribution and rates of N_2 fixation have been inferred at the global scale using several tools. (Deutsch et

73 al., 2007) have introduced the tracer P* which represents the excess of P relative to the standard N quota. A decrease in

74 this tracer is then interpreted as N_2 fixation, since N_2 fixation extracts PO_4 alone. More recently, (Luo et al., 2014)

developed a multiple linear regression that relates N_2 fixation from the MAREDAT database (Luo et al., 2012) to environmental conditions (nutrients, SST, irradiance, MLD,...) in order to build a statistical model for global N_2 fixation distribution. Finally, numerical models have also been used and they allow to overcome the scarcity of observations that may limit the two previous approaches. Indeed, models can be used to investigate the spatial and temporal variability of dinitrogen fixation and to study the controlling environmental factors.

Among those studies focusing on the spatial distribution of dinitrogen fixation, (Berthelot et al., 2017; Bonnet et al., 2009, 2015a; Garcia et al., 2007; Shiozaki et al., 2014) based on oceanographic campaigns have reported high N_2 fixation rates in the Western Tropical South Pacific (WTSP), that has been recently identified as a globally important hot spot of N_2 fixation with rates > 600 µmol N $m^{-2}.d^{-1}$ (Bonnet et al., 2017). Very high abundances of Trichodesmium have been historically reported in this region (Dupouy et al., 2000, 2011; Moisander et al., 2008; Neveux et al., 2006; Shiozaki et al., 2014); Stenegren et al., This issue) and have recently been identified as the major contributor to N_2 fixation in this region (Berthelot et al., 2017); Bonnet et al., This issue). However, the reasons for such an ecological success of diazotrophs in this region are still poorly understood.

In this study, we aim at bringing new insights on this known, but poorly understood, "nitrogen fixation hotspot". This study ambitions to understand the spatial and temporal distribution (i.e. seasonal variability) o*f Trichodesmiu*m and to evaluate the potential impact o*f Trichodesmiu*m fixers on the biogeochemical conditions of the WTSP. We will specifically address the following overarching questions: (i) What are the mechanisms that structure the *Trichodesmium* distribution in the WTSP, particularly around the South West Pacific islands, and (ii) what is the biogeochemical impact of N_2 fixation in this region? Noteworthy, this study is also taking advantage of the sampling done during the OUTPACE cruise, which nicely complement the data coverage in the south west Pacific, and allow a better characterization of the processes responsible for the spatial and seasonal variability of the N_2 fixation.

To fulfill our objectives, we have implemented an explicit representation of the nitrogen fixers in a biogeochemical model, based on the *Trichodesmium* physiology. The first section of this study describes the experimental design and the observation used in our study, while the second part of the paper provides a validation of our reference simulation with an analysis of the *Trichodesmium* compartment and its impacts on the biogeochemical conditions of the Tropical Pacific. In the discussion, the impact of iron from islands sediment on dinitrogen fixation is considered as well as the added value of an explicit dinitrogen fixer compartment rather than a simpler implicit representation of dinitrogen fixation. Finally, implications and limits of our modeling exercise are detailed in the conclusion.

2. Methods

2.1 Coupled dynamical (ROMS)-primary production (PISCES) model

In this study, we used a coupled dynamical-biogeochemical framework based on the regional ocean dynamical model ROMS (Regional Oceanic Modeling System, (Shchepetkin and McWilliams, 2005) and the state of the art biogeochemical model PISCES (Pelagic Interactions Scheme for Carbon and Ecosystem Studies). The ocean model configuration is based on the nested version of ROMS (Penven et al., 2006) and covers the tropical Pacific region [33°S-33°N;110°E-90°W]. It has 41 terrain-following vertical levels with 2-5 m vertical resolution in the top 50 meters of the water column, then 10-20 m resolution in the thermocline and 200-1000 m resolution in the deep ocean. The

114   horizontal resolution is 1°. The turbulent vertical mixing parameterization is based on the non-local K profile

115   parameterization (KPP) of (Large et al., 1994). Open boundary conditions are treated using a mixed active/passive

116   scheme (Marchesiello et al., 2001). This scheme allows to force our regional configuration with large-scale boundary

117   conditions from a ½° global model simulation (details available in (Couvelard et al., 2008), while allowing anomalies to

118   radiate out of the domain. The use of similar ROMS configurations in the WTSP is largely validated through studies

119   demonstrating skills in simulating both the surface (Jullien et al., 2012, 2014; Marchesiello et al., 2010) and subsurface

120   ocean circulation (Couvelard et al., 2008). To compute the momentum and fresh water/heat fluxes, we use a

121   climatological forcing strategy. The momentum forcing is computed from a 1993-1996 7-day climatology of the ERS1-

122   2 scatterometer stress (http://cersat.ifremer.fr/oceanography-from-space/our-domains-of-research/air-sea-interaction/ers-

123   ami-wind). Indeed, ERS derived forcing has been shown to produce adequate simulations of the Pacific Ocean

124   dynamics (e.g, (Cravatte et al., 2007). Heat and fresh water forcing is computed from the COADS climatology 1-day

125   averaged outputs are stored for analysis. ROMS forces on line a biogeochemical model with the noticeable use of a

126   WENO5 advection scheme (i.e. five order weighted essentially non-oscillatory scheme; Shchepetkin and McWilliams,

127   1998).

128   The biogeochemical model PISCES simulates the marine biological productivity and the biogeochemical cycles of

129   carbon and the main nutrients (P, N, Si, Fe) (Aumont and Bopp, 2006a). In PISCES, there are five modeled limiting

130   nutrients for phytoplankton growth: nitrate, ammonium, phosphate, silicate and iron. Those nutrients are delivered to

131   the ocean through dust deposition, river runoff and mobilization from the sediment. In addition to the nutrients,

132   Dissolved Inorganic Carbon (DIC), total alkalinity and dissolved oxygen are also simulated. Three non-living organic

133   compartments are represented: semi-labile dissolved organic matter, small sinking particles, and large sinking particles.

134   In this study, we used a modified version of PISCES which differs in the use of a full quota formulation (with only

135   variable Redfield ratios; (Droop, 1983) rather than the mixed Monod-quota approach (with fixed ratios for nitrogen,

136   phosphorus and silica; Monod, 1942) used in the standard PISCES version (Aumont and Bopp, 2006). In this "quota"

137   version of PISCES (Kwiatkowski et al, 2017, submitted), the phytoplankton growth is limited by the internal

138   availability in nutrients. For the purpose of this study, we also implemented in this quota version an explicit

139   representation of Trichodesmium. Therefore, five living compartments are modeled with three phytoplankton groups

140   (nanophytoplankton, diatoms, and *Trichodesmium*) and two zooplankton groups (microzooplankton, and

141   mesozooplankton).

142   In our configuration, the growth rate of *Trichodesmium* is limited by light, temperature, phosphorus and iron

143   availability. *Trichodesmium* growth rate is computed as follows:

144   Growth rate = ($\mu FixN_2 + \mu TriNO_3 + \mu TriNH_4$),

145   where $\mu FixN_2$ denotes growth due to dinitrogen fixation, $\mu TriNO_3$ and $\mu TriNH_4$ represent growth sustained by NO_3^- and

146   NH_4^+ uptake, respectively. Dinitrogen fixation is activated when reactive nitrogen species are limiting. Otherwise,

147   *Trichodesmium* grows on NO_3^- and NH_4^+ just like standard nanophytoplankton do. Moreover, a fraction of fixed

148   nitrogen is released by the simulated Trichodesmium. (Berthelot et al., 2015) estimated this fraction at less than 10%

149   while considering all diazotrophs. Because we are only representing Trichodesmium, we set up this fraction at 5% of

150   total amount of fixed nitrogen.

151   Dinitrogen fixation is controlled by the availability of phosphate, iron and light and is modulated by temperature. The

152   complete set of equations of *Trichodesmium* is detailed in Appendix 1. This setup reproduces the dinitrogen fixation

153   through an explicit representation of the Trichodesmium biomass (to be compared with often used implicit

154   parameterization that links directly environmental parameters to nitrogen fixation without requiring the Trichodesmium

155 biomass to be simulated).

156

2.2 Setup of experiments

158

159 Below are summarized the set of experiments that have been performed in this study (Table 1). A first simulation over
160 20-years (1993-2013) has been performed as a reference experiment, hereafter referred to as "TRI". This reference
161 simulation uses the explicit dinitrogen fixation module described above. In a second experiment called
162 "TRI_NoFeSed", the model setup is identical to the reference experiment, except that iron input from the sediments is
163 turned off between 156°E and 240°E. In a third experiment "N2_imp", the explicit dinitrogen fixation module is
164 replaced by the implicit parameterization described in (Aumont et al., 2015). Finally, a fourth experiment "N2_Wo"
165 corresponds to a model setup in which no explicit nor implicit description of dinitrogen fixation is activated.
166 Comparison between TRI and TRI_NoFeSed experiments allow to estimate the impact of iron input from island
167 sediments on the dinitrogen fixation, while the impact of dinitrogen fixation on the biogeochemical conditions in the
168 Pacific Ocean can be investigated by comparing TRI and N2_Wo. Finally, the TRI and N2_imp experiments are used to
169 evaluate the added value of an explicit description of dinitrogen fixation relative to an implicit inexpensive
170 parameterization.

171

2.3 Observational datasets.

173

174 Several different databases have been used to evaluate the model skills. For nitrate and phosphate, the CSIRO ½°
175 global Atlas of Regional Seas (CARS, http://www.marine.csiro.au/~dunn/cars2009/) has been used. Iron has been
176 evaluated with the global database from (Tagliabue et al., 2012), to which the dissolved iron data from the OUTPACE
177 cruise (Guieu et al., under review) have been added. This database is a compilation of 13125 dissolved iron
178 observations covering the global ocean and encompassing the period 1978–2008. The global MARine Ecosytem DATa
179 (MAREDAT, https://doi.pangaea.de/10.1594/PANGAEA.793246) database of N_2 fixation has been expanded with data
180 from recent cruises performed in the WTSP (MOORSPICE, (Berthelot et al., 2017), DIAPALIS ((Garcia et al., 2007),
181 NECTALIS (http://www.spc.int/oceanfish/en/ofpsection/ema/biological-research/nectalis), PANDORA (Bonnet et al.,
182 2015a), OUTPACE (Bonnet et al., This issue), Mirai (Shiozaki et al., 2014) has been used for dinitrogen fixation rates.
183 This database contains 3079 data points at the global ocean scale, of which ~1300 are located in our simulation region
184 (Luo et al., 2012). Finally, we have used surface chlorophyll concentrations from the GLOBCOLOUR project
185 (http://ftp.acri.fr) which spans the 1998-2013 time period.

186

3.Results

3.1 Model Validation

189

190 In this subsection, we aim at validating our reference simulation "TRI" with the data previously mentioned. In the
191 Pacific, phosphate and nitrate concentrations show maxima in the upwelling regions, i.e. along the western American
192 coast, and in the equatorial upwelling (Fig. 1a,c), and mimima in the subtropical gyres. First, phosphate patterns show

193   modeled values and structures in qualitatively good agreement with observations. In contrast, the nitrate structure shows

194   some biases. We observe concentrations higher than 1 μmol.L^{-1} all along the equator in CARS, while in the model

195   nitrate concentrations are lower than this value west of 170W°. More generally the model tends to underestimate nitrate

196   concentrations.

197   The regions most favorable for *Trichodesmium* can be defined by temperature within 26-29°C. The model reproduces

198   relatively well the spatial distribution of this temperature preferendum. This distribution exhibits a significant seasonal

199   variability, mainly as a result of the variability of the 26°C isotherm. The latter moves by ~5° latitudinally between

200   summer and winter in the WTSP, and by ~15° in the Western Tropical North Pacific (WTNP) (Fig. 1a). Along the

201   equator, this isotherm migrates by 15° eastward during summer (Fig. 1a). This temporal variability is well reproduced

202   by the model (Fig. 1b). In contrast, nitrate and phosphate seasonal variability remains low (not shown).

203   Another important feature that needs to be properly reproduced by the model is the iron distribution in the upper ocean.

204   The median value as well as the dispersion of the iron surface concentrations over the tropical Pacific, are displayed for

205   both the data and the model in Figure 2a. No statistical differences can be distinguished, the model being sampled at the

206   same time and same location as the data. This latter result shows a good agreement between the data and the model at

207   the tropical Pacific scale (Fig 2b compared to Fig. 2c). The best sampled area is the central Pacific ocean where

208   simulated iron concentrations are low (0.1 to 0.3 nmol Fe.L^{-1}), which is consistent with the observations. The southwest

209   Pacific is characterized by relatively high surface iron concentrations, between 0.4 and 0.8 nmol Fe.L^{-1}, both in the data

210   and in the model. Large scale patterns are thus well represented by the model. Nevertheless, the model tends to

211   overestimate iron levels in the south Pacific gyre, between 180° and 140°W at about 20°S.

212   Figure 3 displays a comparison between surface Chlorophyll concentrations from GLOBCOLOUR data (a), and from

213   TRI (b) and TRI_imp (c) simulations. Strong chlorophyll concentrations are found in the eastern equatorial Pacific

214   upwelling and along Peru in both the observations and our 2 simulations, with mean values of 0.3 mg Chl.m^{-3}. The

215   equatorial rich tongue simulated by the model (Fig. 3b,c) is however too narrow compared to the observations,

216   especially in the northern hemisphere. Similarly, the model is unable to simulate the elevated chlorophyll levels around

217   the Costa Rica dome and the localized enhanced chlorophyll off Papua New Guinea. In TRI (Fig. 3b), chlorophyll

218   values in the South West Pacific region vary between 0.1 and 0.2 mg Chl.m^{-3}, with maxima located in the vicinity of the

219   Fiji and Vanuatu islands. These values are within the range of the data, even if the data tend to be slightly higher (up to

220   0.3 mg Chl.m^{-3} near the coasts). The spatial structure is well represented, with maxima simulated around the islands.

221   Those localized chlorophyll enhancement suggest a specific island effect. In the subtropical gyres, the simulation

222   predicts chlorophyll concentrations of ~0.05 mg Chl.m^{-3} which are higher than the observations (< 0.025 mg Chl.m^{-3}).

223   In contrast in TRI_imp (Fig. 3c), chlorophyll values in the South West Pacific and in the North hemisphere are too low

224   in comparison with the ocean colour data (Fig. 3a). TRI simulation thus appears in better agreement with the

225   observations than TRI_imp.

226   Part of the surface chlorophyll in Figure 3b is associated to *Trichodesmium*. The Figure 3d shows the annual mean

227   spatial distribution of surface Trichodesmium chlorophyll in the "TRI" simulation. This distribution displays two zonal

228   tongues in the tropics, one in each hemisphere. Maximum values are located in the South West Pacific (around Vanuatu

229   archipelago, New Caledonia, Fiji, and Papua New Guinea) and around Hawaii, where they reach 0.06 mg Chl.m^{-3}. In

230   the south Pacific, high chlorophyll biomass extends eastward until 130°W. Further east, concentrations drop to below

231   0.02 mg Chl.m^{-3}. It's important to note that in the observations *Trichodesmium* has never observed beyond 170°W. This

232   bias in the model could be explain by the overestimation of iron concentrations in SPG. In the Northern Hemisphere,

233   between the coast of Philippines (120°E) and Hawaii (140°W), *Trichodesmium* chlorophyll concentrations are greater

234   than 0.03 mg Chl.m^{-3}. In the North East Pacific, *Trichodesmium* chlorophyll is lower, yet significant (<0.03 mg Chl.m^{-3}).

235   Otherwise the equatorial Pacific and South-east Pacific oceans are overall poor in *Trichodesmium*.

236   In Figure 4, the dinitrogen fixation rates predicted by the model in "TRI" are compared to the observations from the

237   MAREDAT expanded database. Evaluation of the model behavior remains quite challenging because of the scarcity of

238   the observations. Some large areas are not properly sampled such as the north west tropical Pacific and the eastern

239   Pacific. Nevertheless, some regional patterns emerge from the observations. Maximum fixation rates (~600 to 1600

240   µmol N.m^{-2}.d^{-1}; Fig. 4a) are observed around the south west Pacific islands, in the Solomon Sea, around the Melanesian

241   archipelagoes and around Hawaii, four well known « hotspots » of N$_2$ fixation (Berthelot et al., 2015, 2017, Bonnet et

242   al., 2009, 2017; Böttjer et al., 2017). The modeled regional patterns of strong fixation are coherent with the observations

243   (Fig. 4b), showing values in the same range. In the south Pacific, the TRI simulation is able to reproduce the strong

244   east-west increasing gradient of N$_2$ fixation as reported by dinitrogen fixation (Shiozaki et al., 2014; Bonnet et al., This

245   issue; Fig 4c,d). In the equatorial Central Pacific, modeled values of mean fixation are negligible (< 0.5 µmol N.m^{-2}.d^{-1})

246   in contrast to the observations which suggest low but non-negligible fixation rates (between 1 to 2 µmol N.m^{-2}.d^{-1};

247   (Bonnet et al., 2009; Halm et al., 2012). In general, dinitrogen fixation rates are overestimated by ~70% in TRI

248   compared to the data. Some recent studies have shown that the ^{15}N$_2$-tracer addition method (Montoya et al., 2004) used

249   in most studies reported in the MAREDAT database may underestimate N$_2$ fixation rates due to an incomplete

250   equilibration of the ^{15}N$_2$ tracer in the incubation bottles, which may explain the differences observed between the

251   modeled and measured rates (Großkopf et al., 2012; Mohr et al., 2010). However, some other studies performed in the

252   South Pacific (Bonnet et al., 2016b; Shiozaki et al., 2015) compared the two methods, and did not found any significant

253   differences.

254

3.2 Trichodesmium Primary Production

256   We evaluated the direct relative contribution of *Trichodesmium* to PP (Fig. 6). The spatial distribution of this

257   contribution is very similar to the spatial distribution of *Trichodesmium* chlorophyll, with 2 distinct tongues located on

258   each side of the Equator in the tropical domain. In the Northern hemisphere, the tongue extends from the coast of

259   Philippines (120°E) to Hawaii (140°W) longitudinally and between 10°N and 25°N latitudinally. The maximum

260   contribution (~35%) is reached near Hawaii while in the rest of the tongue, values are close to 20%. In the Southern

261   Hemisphere, the region of elevated contribution extends from PNG (140°E) to about the center of the South Pacific

262   subtropical gyre at 130°W, and between 5°S and 25°S latitudinally. Maximum values are predicted in the vicinity of

263   Vanuatu and Fiji Islands, where they can reach 35%. Part of this elevated contribution is explained by the very low PP

264   rates simulated in this region for both nanophytoplankton and diatoms (less than 0.03 mol C.m^{-3}.yr^{-1}). Furthermore, the

265   island effect seems to represent an important factor for explaining the spatial distribution of *Trichodesmium* growth

266   rates. Indeed, maximum *Trichodesmium* chlorophyll concentrations and the largest contribution of *Trichodesmium* to PP

267   are achieved near the islands. Finally, in LNLC regions (red boxes; fig. 1c,d), we assess that *Trichodesmium* contribute

268   to 15% of total PP, which is in accordance with biogeochemical studies performed in these areas (Bonnet et al., 2015;

269   Berthelot et al., 2017; Caffin et al., This issue)

270

3.3 Seasonal variability of Trichodesmium biomass

272   Simulated dinitrogen fixation rates and *Trichodesmium* biomass (not shown) display a seasonal variability that is driven

273 by the seasonal variability of the environmental conditions (light, temperature, currents, nutrients). The regional

274 maxima of *Trichodesmium* biomass (exceeding 3 mmol C.m^{-2}; integrated over the top 100m of the ocean) are found in

275 both hemispheres during the summer season (Fig. 7a,e) even if locally, maxima can be attained during other periods of

276 the year than summer. In the south Pacific, the area of elevated *Trichodesmium* biomass moves by 3° southward from

277 austral winter to austral summer. Along Australia and in the Coral Sea, *Trichodesmium* biomass exhibits a large seasonal

278 variability with very low winter biomass that contrast with elevated values in summer. A similar important variability,

279 which is shifted by six months, is simulated in the Northern hemisphere in the Micronesia region and in the Philippine

280 Sea.

281 Unfortunately, due to the scarcity of N$_2$ fixation data over the annual cycle, this seasonal cycle cannot be properly

282 assessed at the scale of the tropical Pacific Ocean. This is only feasible at the time series station ALOHA located in the

283 North Pacific gyre at 22°45',158°W, where seasonal data of dinitrogen fixation are available from 2005 to 2012 (Böttjer

284 et al., 2017). They proved that vertically integrated dinitrogen fixation rates are statistically significantly lower from

285 November to March (less than 200 μmol N m^{-2}.d^{-1}) than from April to October (about 263 ± 147 μmol N.m^{-2}.d^{-1}) as

286 highlighted in Figure 5a (blue dots). In the model (red dots; Fig. 5a), the maximum amplitude of the seasonal cycle

287 appears to be underestimated relative to the observations (i.e. respectively ~170 μmol N.m^{-2}.d^{-1} and ~250 μmol N.m^{-2}.d^{-1}

288 $^{-1}$). Dinitrogen fixation peaks one month earlier in the model than in the data (August for the model and September for

289 the data). The simulated dinitrogen fixation rates are minimum between December and May (averaging $\sim241 \pm 27$

290 μmol N.m^{-2}.d^{-1}) and maximum the rest of the year (averaging $\sim 347 \pm 52$ μmol N.m^{-2}.d^{-1}). These values are comparable

291 to the data even if they are slightly higher.

292 In order to assess the seasonal cycle of N$_2$ fixation rates in the south Pacific (red box Fig 1c; 160°E-230°E; 25°S-14°S),

293 we have extracted the available data for each month from our database (blue dots; Fig. 5b), and the corresponding

294 model values in TRI (red dots; Fig 5b). In July no observations are available and in January, April and August, only one

295 data point is available for the entire region. The predicted seasonal cycle is broadly consistent with observations.

296 Minimum dinitrogen fixation rates (239 ± 205 μmol N.m^{-2}.d^{-1}) occur during austral winter and autumn. Maximum rates

297 are reached in February and March, where they exceed 600 μmol N.m^{-2}.d^{-1} in the observations. The increase in

298 dinitrogen fixations rates occurs one month earlier than in the observations, in December instead of January, and

299 remains two to three fold higher from April to June. It is important to note here that the sampling spatial and temporal

300 distribution may distort the seasonal cycle. Using the model, it is possible to evaluate how well the seasonal cycle is

301 captured by the sampling (red dots compared to green dots; Figure 5b). The general structure of the seasonal cycle

302 remains relatively unaltered. However, the amplitude is significantly impacted since it reaches 1100 μmol N.m^{-2}.d^{-1} in

303 the sampling whereas it is about twice as low at 600 μmol N.m^{-2}.d^{-1} when all the model data points are considered. We

304 can conclude that the TRI simulation reproduces well the seasonal cycle of N$_2$ fixation rates at the Pacific scale, even

305 though more data are needed to improve the evaluation of the model skills.

306 To further investigate the mechanisms that drive the seasonal variability of *Trichodesmium* in the Pacific, we examined

307 the factors that control Trichodesmium abundance in the TRI simulation (not shown). This analysis indicates that this

308 seasonal variability is mainly controlled by primary production. Hence we further examine the limitation terms of

309 primary production (Fig. 8) in two representative regions characterized by elevated levels of N$_2$ fixation rates (red

310 boxes; Fig 1c). A detailed description of these limitation terms is given in Appendix 1. A limitation term reaching 1

311 means that growth is not limited whereas a limitation term equal to zero means that growth ceases.

312 *Trichodesmium* growth sustained by nitrate and ammonia is very small in LNLC regions due to their very low

313 availability and is therefore not considered further. Thus, our analysis is restricted to dinitrogen fixation. *Trichodesmium*

314   growth can be limited by iron and phosphate and is inhibited when reactive nitrogen (nitrate and ammonia) is available.
315   In the WTSP, the model suggests that iron is the sole nutrient that modulat*es* Trichodesmium growth (red curve; Fig.
316   8a,b). The others limiting factors *of Trichodesm*ium growth are light (green curve; Fig 8a,b) and temperature (purple
317   curve; Fig. 8a,b). The product of these 3 limiting factors gives the limiting coefficient of dinitrogen fixation (brown
318   curve; Fig. 8a,b). The limiting factors vary according to the season and the hemisphere. In the south (north) Pacific,
319   temperature and light are less limiting during the austral summer (winter) than during the austral winter (summer). The
320   limiting factor associated to temperature varies from 0.8 to 1, and the light limiting factor varies from 0.15 to 0.3.
321   Unlike light and temperature, iron is less (more) limiting in the south (north) pacific during winter (summer) than
322   during the austral summer (winter) with values varying between 0.4 and 0.7. Finally, *Trichodesmium* growth is more
323   limited during the austral winter (summer) in the south (north) Pacific. The seasonal variability is forced by light and
324   temperature, and iron mitigates its amplitude. Indeed, temperature and iron are anti-correlated because, in the boxes
325   over which this analysis is performed, the ocean dynamic is mainly 1D. Nutrients are thus brought by enhanced vertical
326   mixing which also cools temperature.

4. Discussion

330   The implementation of dinitrogen fixation in ocean models has become more and more complex over the past twenty
331   years. At first, the supply of new nitrogen by dinitrogen fixation has been embedded into models by developing implicit
332   parameterizations (Bissett et al., 1999). Subsequently explicit descriptions of diazotrophs have been developed, mainly
333   based on the knowledge derived from laboratory experiments focused on Trichodesmium sp. (Fennel et al., 2001; Hood
334   et al., 2001; Moore et al., 2001). Since the mid-2000s, studies focused on the role of iron in controlling the distribution
335   of diazotrophs and dinitrogen fixation (Keith Moore et al., 2006; Krishnamurthy et al., 2009; Moore et al., 2004;
336   Tagliabue et al., 2008).

4.1 Impact of iron from island sediments

340   Monteiro et al. (2011) and Dutkiewicz et al. (2012) have suggested that a realistic representation of marine iron
341   concentration is key to simulate the diazotrophs habitat. Monteiro et al. (2011) performed a sensitivity study and found
342   that a fivefold increase in the solubility of aeolian iron improves the biogeographical distribution of N_2 fixation in the
343   southwest Pacific. In the meantime, a recent study has challenged this view by showing no increase in dinitrogen
344   fixation in response to increased dust deposition (Luo et al., 2014). In any cases, the sedimentary and hydrothermal
345   sources were not taken into account in those studies, although they are likely significant sources (Bennett et al., 2008;
346   Johnson et al., 1999; Moore et al., 2004; Tagliabue et al., 2010; Toner et al., 2009). In parallel, Dutkiewicz et al. (2012)
347   evaluated the sensitivity of the biogeographical distribution of N_2 fixation to the aeolian source of iron in a model which
348   takes into account the iron sediment supplies, and conclude for minor changes in south west Pacific, while in the north
349   Pacific the change was larger. Indeed, there are many high islands that could deliver significant amounts of iron to the
350   ocean (Radic et al., 2011) in the southwest Pacific.
351   To assess the impact of the sediment source of iron on the *Trichodesmium* production, we used the "TRI_NoFeSed"
352   experiment in which this specific source of iron has been turned off for the islands between 160°E and 120°W (Table 1).

353 In this simulation, the iron and the *Trichodesmium* chlorophyll concentrations decrease by 58% and 51% respectively

354 (Fig. 9a,b), in the WTSP (red box Fig 1c). Figure 9c displays the iron distribution simulated in TRI_NoFeSed, and

355 shows that the maximums around the islands disappear. Furthermore, in the south Pacific, iron decreases due to the

356 reduction of the zonal advection of iron downstream of the islands. The iron flux from the sediments around the islands

357 also affects the spatial structure of *Trichodesmium* chlorophyll (Fig. 9d,e), most noticeably in the south Pacific, with

358 maxima shifted from the south Pacific islands region (e.g. Fiji, New Caledonia, Vanuatu) in the TRI simulation to the

359 coastal regions near Australia and Papua New Guinea in the TRI_NoFeSed simulation. In the northern hemisphere, the

360 effects of the sediment flux of iron are less important with a shift of the *Trichodesmium* chlorophyll maxima towards the

361 Philippine Sea and a localized effect near Hawaii. This sensitivity test demonstrates that *Trichodesmium* are highly

362 sensitive to the iron distribution in our model and hence that the spatial patterns of *Trichodesmium* chlorophyll in the

363 south west Pacific are tightly controlled by the release of iron from the coastal sediments of the Pacific islands.

364

4.2 *Trichodesmium* impacts on biogeochemistry

366

367 One of the questions we want to address is the quantification of the *Trichodesmium* impact on primary production (PP),

368 at the Pacific scale with a focus on the WTSP region. In the oligotrophic waters of the south pacific, dinitrogen fixation

369 can be an important source of bio-available nitrogen in the water column through *Trichodesmium* recycling which can

370 feed other phytoplankton. To evaluate that impact, we calculated the relative increase of PP between the TRI simulation

371 and the N2_Wo simulation in which no dinitrogen fixation is considered (Fig 10a). As expected, the spatial structure of

372 the primary production differences between both simulations matches the dinitrogen fixation spatial distribution in the

373 TRI simulation (two tongues, one in each hemisphere). In the north Pacific the maximum increase of the primary

374 production due to the dinitrogen fixation is located around Hawaii, where it exceeds 120%. In the remaining part of the

375 northern hemisphere tongue, primary production increases by 50% to 100%. In the southern hemisphere, values are

376 more homogeneous in the tongue (from 80 to 100%), even though there is a local maximum around Fiji and Vanuatu

377 (up to 120%). Out of these northern and southern tongues, the increase of PP is less than 20%. In average on our

378 domain, the increase of PP is 19% and in LNLC regions, it reaches approximately 50%.

379 From total primary production only, it is not possible to disentangle the increase of primary production directly due to

380 *Trichodesmium* themselves and the indirect increase due to the impact of dinitrogen fixation on the other phytoplankton

381 groups (nanophytoplankton and diatoms). Indeed, as mentioned in the method section, *Trichodesmium* also releases a

382 fraction of the recently fixed N_2 as bio-available nitrogen (mostly ammonia and dissolved organic nitrogen). Figure 10b

383 displays the difference of PP due to diatoms and nanophytoplankton only. The main large scale patterns constituted of

384 the northern and southern tongues persist, but the intensity of the differences contrasts with those found when

385 considering total primary production (Fig. 10a). Indeed, the increase of total primary production (Fig 10a) in those two

386 tongues is twice as high as when the direct effect *of Trichodesm*ium is excluded. This analysis stresses the importance of

387 the bio-available nitrogen released by diazotrophs as we attribute about half of the total production increase to this

388 release. Indeed, recent isotopic studies tracing the passage of diazotroph-derived nitrogen into the planktonic food web

389 reveal that part of the recently fixed nitrogen is released to the dissolved pool and quickly taken up (24-48%) by

390 surrounding planktonic communities (Berthelot et al., 2016; Bonnet et al., 2016a, 2016b)).

391 With the simulation N2_imp, we aim at comparing an implicit dinitrogen fixation formulation to the explicit

392 formulation used in TRI. Figure 10c displays the relative change of total PP between the TRI and the N2_imp

393   simulations (see Table 2). The implicit formulation displays a similar spatial distribution than the explicit distribution

394   but is predicting a lower total primary production, especially in the the southern Pacific where explicit formulation

395   leads to an increase of about 45% in total PP compared to the one related to the implicit formulation. On average across

396   our domain, total primary production is about ~ 9% higher when nitrogen fixation is explicitly modeled relative to an

397   implicit formulation.

398   This difference becomes even weaker (2%) if only primary production by nanophytoplankton and diatoms is

399   considered, with noticeable differences restricted to the areas of maximum dinitrogen fixation in the southern

400   hemisphere (around the islands). PP sustained by the release of bio-available nitrogen is thus similar in the TRI and

401   N2_imp simulations, but an explicit representation of dinitrogen fixation allows a better description of dinitrogen

402   fixation patterns. Indeed, the areas of intense dinitrogen fixation rates cannot be properly simulated in the vicinity of the

403   islands, especially in the southern hemisphere, by the tested implicit parameterization.

404

405   **4.3 Limitations**

406

407   In this study, we simulate dinitrogen fixation through the explicit representation of only one type of diazotrophs, the

408   *Trichodesmium* sp. This choice has been motivated by evidences that it represents one of the main nitrogen fixers in the

409   western tropical Pacific (Bonnet et al., 2015a; Dupouy et al., 2011; Shiozaki et al., 2014) and by the relatively good

410   knowledge (compared to other dinitrogen fixers) we have about its physiology (Ramamurthy and Krishnamurthy, 1967;

411   Ohki et al., 1992; Mulholland and Capone, 2000; Mulholland et al., 2001; Küpper et al., 2008; Rubin et al., 2011;

412   Bergman et al., 2013). However, our model remains simple and some of the mechanisms that drive the behavior of

413   *Trichodesmium* have not been implemented in our model. As an example, the ability of *Trichodesmium* to group in

414   colonies and to vertically migrate (Kromkamp and Walsby, 1992; Villareal and Carpenter, 2003; Bergman et al., 2013)

415   (Bergman et al., 2013; Kromkamp and Walsby, 1992; Villareal and Carpenter, 2003) is well documented. The reason of

416   these mechanisms remains unclear, but several hypotheses have been put forward such as avoiding nitrogenase

417   exposition to di-oxygen (Carpenter, 1972; Gallon, 1992; Paerl et al., 1989), or maximizing light (on the surface) and

418   nutrients (at depth) acquisition (Letelier and Karl, 1998; Villareal and Carpenter, 1990; White et al., 2006), or even

419   increasing the efficiency of the uptake of atmospheric iron (Rubin et al., 2011). Our model does not represent those

420   processes, nor does it model the resulting vertical migration of *Trichodesmium*. Moreover, the release of fixed

421   dinitrogen as reactive nitrogen bioavailable to other phytoplanktonic organisms has been set to a constant value of 5%.

422   This percentage is known to be highly variable and therefore this value is in the lowest range of the observations. An

423   increase in this value would increase the PP due to nanophytoplankton and diatoms in the TRI simulation, and thus

424   decrease the relative contribution of Trichodesmium to total PP, which would be closer to the last observations

425   (Berthelot et al. 2017; Bonnet et al. 2017).

426   Some studies, mostly based on extrapolated in-situ data, aimed at assessing the potential of dinitrogen fixation at global

427   or regional scale (Codispoti et al., 2001; Deutsch et al., 2001; Galloway et al., 2004). In the western south tropical

428   Pacific, Bonnet et al (2017) have estimated total nitrogen fixation at 15 to 19 Tg N.yr^{-1}. For the same region, nitrogen

429   fixation is predicted to amount to ~7 Tg N.yr^{-1} in the TRI simulation. As already mentioned, this rather low predicted

430   estimates might be explained by the sole representation of Trichodesmium as nitrogen fixing organisms, which

431   dominate in the western tropical south Pacific (Dupouy et al., 2011, Stenegren et al., This issue). It has to be noted that

432   other diazotroph groups such UCYN-B and DDAs are abundant in the WTSP, representing 10-20% of the overall

433   diazotroph community (Stenegren et al., This issue). Moreover, the contribution of heterotrophic diazotrophic organism

434   is poorly studied and may account for a significant fraction of N_2 fixation (Moisander et al., 2017). Our model

435   estimation has also been computed from monthly averages and is thus not taking into account the high-frequency

436   variability that may explain at least some of the very high rates of dinitrogen fixation used in the study by Bonnet et al.

437   (2017). Our assessment based on a model could thus be seen as a lower limit for dinitrogen fixation in the western

438   tropical Pacific. Moreover, our model shows also a good qualitative agreement with the studies based on observations

439   that focus on the impact of dinitrogen fixation in tropical oligotrophic waters (Raimbault and Garcia, 2008; Shiozaki et

440   al., 2013). Indeed, in agreement with those studies, our reference simulation predicts that diazotrophs support a large

441   part of PP (~ 15%) in LNLC regions.

442   **5. Conclusion**

443   This study describes the spatial and temporal distribution of *Trichodesmium* at the scale of the tropical Pacific ocean,

444   and investigates the impact of a major diazotroph species (e.g *Trichodesmium* sp.) on the biogeochemistry of this

445   region. Toward this end, we performed a first 20-year simulation with the coupled 3D dynamical biogeochemical model

446   ROMS-PISCES in which we embedded an explicit representation of dinitrogen fixation based on *Trichodesmium*

447   physiology. This simulation was shown to be able to reproduce the main physical (SST) and biogeochemical (nutrients)

448   conditions of the tropical Pacific ocean. This includes the spatial distribution of surface chlorophyll and dinitrogen

449   fixation.

450   The validation of this simulation allows us to confidently assess the *Trichodesmium* distribution. The model predicts

451   that areas favorable to *Trichodesmium* growth extend from 150°E to 120°W in the south Pacific, and from 120°E to

452   140°W in the north Pacific, with local optimal conditions around the islands (i.e., Hawaii, Fiji, Samoa, New Caledonia,

453   Vanuatu). This broadly corresponds to the LNLC regions where Trichodesmium are predicted to be responsible for

454   15% of total primary production. The seasonal variability of the Trichodesmium habitat is dominantly controlled by

455   SST and light, while iron availability modulates the amplitude of the seasonal cycle.

456   In our study we also assess the role played by iron released from the island sediments, and show that this iron source

457   partly controls the spatial structure and the abundance of *Trichodesmium* in the western tropical south Pacific. However,

458   this region is in the center of the south Pacific convergence zone which is the largest convective area of the Southern

459   Hemisphere, with rainfall exceeding 6mm.day^{-1}, hence it would be interesting to assess the impact of river iron supply

460   on the diazotrophs activity. In addition, the Vanuatu archipelago and Tonga are located on the ring fire, hence

461   hydrothermal sources could have a strong impact on dinitrogen fixation. These two iron sources are not yet

462   implemented in our configuration but may improve simulations of dinitrogen fixation in the south western tropical

463   Pacific region.Finally, our explicit simulation of dinitrogen fixation has proven to be higher by 25% (while still in the

464   lower end of estimations from observations) than the more commonly used implicit parameterization.

465

466   **6. Appendix**

467

468   *Trichodesmium* preferentially fixes di-nitrogen at temperature between 20-34°C (Breitbarth et al., 2008). The

469   temperature effect on the growth rate is modeled using a 4th order polynomial function (Ye et al., 2012):

470

471 $$L_T^{Tri} = \frac{2,32.10^{-5} \times T^4 - 2,52.10^{-3} \times T^3 + 9,75.10^{-2} \times T^2 - 1,58 \times T + 9.12}{0.25}$$

472

473 where $0.25 d^{-1}$ is the maximum observed growth rate (Breitbarth et al., 2008). Hence, at 17°C the growth rate is zero

474 and maximum growth rate is reached at 27.5°C.

475

476 We first evaluate if nitrate+ammonium limitation occurs. In that case, dinitrogen fixation can occur and it is limited by

477 phosphorus and iron. Phosphorus and iron limitations (L^P, L^{Fe}) are calculated in a 2-step process as follows:

478 First, we determine the most limiting nutrient:

479 $$L_{Tri}^{Fe} = \frac{\left(\theta^{Fe} - \theta_0^{Fe}\right)\theta_{opt}^{Fe}}{\left(\theta_{opt}^{Fe} - \theta_0^{Fe}\right)\theta^{Fe}} \quad \text{and} \quad L_{Tri}^{P} = \frac{\left(\theta^{P} - \theta_{min}^{P}\right)\theta_{opt}^{P}}{\left(\theta_{opt}^{P} - \theta_{min}^{P}\right)\theta^{P}} ,$$

480 where $\theta^{Nutrients}$ represents the nutrient quota for Fe and PO_4 (i.e, the ratio between iron and carbon concentrations in

481 *Trichodesmium*, for instance).

482

483 $$\theta_0^{Fe} = \theta_{min}^{Fe} - m ,$$

484 where m represents the maintenance iron, the intracellular Fe : C present in the cell at zero net growth rate (Kustka et

485 al., 2003).

486

487 θ_{min}^{Nut} and θ_{opt}^{Nut} are constant, whereas θ varies with time. The mimimum of L^{Fe}_{Tri} and L^{P}_{Tri} defines the limiting nutrient.

488 We then evaluate dinitrogen fixation as follows:

489

490 If iron is limiting :

491

492 $$\mu_{FixN_2} = \mu_{max}^{Tri} L_I \frac{\left(\theta^{Fe} - \theta_0^{Fe}\right)\theta_{opt}^{Fe} - L_{Tri}^{N}\left(\theta_{opt}^{Fe} - \theta_0^{Fe}\right)\theta^{Fe}}{\alpha\mu_{max}^{Tri}\theta_{opt}^{Fe} + \left(\theta_{opt}^{Fe} - \theta_0^{Fe}\right)\theta^{Fe}}$$

493 μ_{FixN2} is the growth rate of Trichodesmium sustained by dinitrogen fixation.

494

495 else if phosphorus is limiting :

496 $$\mu_{fixN_2} = \mu_{max}^{Tri} L_I L_P^{Tri} - \left(\mu_{NO_3}^{Tri} + \mu_{NH_4}^{Tri}\right)$$

497

498 which allows to recalculate the actual iron limitation for *Trichodesmium* as follows

499 $$L_{Tri}^{Fe} = \frac{\left(\theta^{Fe} - \theta_0^{Fe} - \alpha\mu_{fixN_2}\right)\theta_{opt}^{Fe}}{\left(\theta_{opt}^{Fe} - \theta_0^{Fe}\right)\theta^{Fe}} ; \alpha = \frac{1}{\beta}$$

500

501 β is the marginal use efficiency and equals the moles of additional carbon fixed per additional mole of intracellular iron

502 per day (Raven, 1988; Sunda and Huntsman, 1997).

503

504 Such recalculation takes into account the fact that Trichodesmium need much higher cell Fe : C ratios to achieve the

505 same growth rate as if growning on ammonium. That limitation is similar to the previous iron michaelis-menten-type

506 limitation except that the growth rate is zero as long as the Fe : C ratio does not reach 14μmol Fe : mol C (Kustka et al.,

507 2003).

508

509 To summarize *Trichodesmium* growth rate:

510

511 If $\mu_{FixN_2} = 0$: $\quad \mu_{NO_3}^{Tri} = \mu_{max}^{Tri} L_I L_P^{Tri} \dfrac{L_{NO_3}^{Tri}}{L_{NO_3}^{Tri} + L_{NH_4}^{Tri}}$ and $\mu_{NH_4}^{Tri} = \mu_{max}^{Tri} L_I L_P^{Tri} \dfrac{L_{NH_4}^{Tri}}{L_{NO_3}^{Tri} + L_{NH_4}^{Tri}}$

512

513

514 If $\mu_{FixN_2} > 0$: $\quad \mu_{NO_3}^{Tri} = \mu_{max}^{Tri} L_I L_{NO_3}^{Tri} min\left(L_P^{Tri}, L_{Fe}^{Tri} \right)$ and $\mu_{NH_4}^{Tri} = \mu_{max}^{Tri} L_I L_{NH_4}^{Tri} min\left(L_P^{Tri}, L_{Fe}^{Tri} \right)$,

515

516

517 L_P^{Tri} , L_N^{Tri}, L_{Fe}^{Tri} are respectively the *Trichodesmium* limiting function by phosphate, nitrogen and iron. L_I is the

518 *Trichodesmium* limiting function by temperature and light.

519 μ_{max}^{Tri} is the *Trichodesmium* maximum growth rate,

520

521 μ_{NO3}^{Tri} and μ_{NH4}^{Tri} are respectively the new and regenerated productions.

522

523 **Acknowledgements**

524 We thank the ship captains, the scientists as well as funding agencies of all the projects (OUTPACE, BIOSOPE,

525 MOORSPICE, DIAPALIS , NECTALIS, PANDORA, Mirai) that allowed data collection without which we could not

526 validate our model. The authors thank Institute of Research for Development for supporting all authors. Cyril Dutheil is

527 funded by European project INTEGRE.

528

529 **Reference**s

530 Arrigo, K. R.: Marine microorganisms and global nutrient cycles, Nature, 437(7057), 349–355,

531 doi:10.1038/nature04159, 2005.

532 Aumont, O. and Bopp, L.: Globalizing results from ocean in situ iron fertilization studies: globalizing iron fertilization,

533 Glob. Biogeochem. Cycles, 20(2), n/a-n/a, doi:10.1029/2005GB002591, 2006b.

534 Aumont, O., Ethé, C., Tagliabue, A., Bopp, L. and Gehlen, M.: PISCES-v2: an ocean biogeochemical model for carbon

535 and ecosystem studies, Geosci. Model Dev. Discuss., 8(2), 1375–1509, doi:10.5194/gmdd-8-1375-2015, 2015.

536 Bennett, S. A., Achterberg, E. P., Connelly, D. P., Statham, P. J., Fones, G. R. and German, C. R.: The distribution and

537 stabilisation of dissolved Fe in deep-sea hydrothermal plumes, Earth Planet. Sci. Lett., 270(3–4), 157–167,

538 doi:10.1016/j.epsl.2008.01.048, 2008.

539 Bergman, B., Sandh, G., Lin, S., Larsson, J. and Carpenter, E. J.: Trichodesmium – a widespread marine

540   cyanobacterium with unusual nitrogen fixation properties, FEMS Microbiol. Rev., 37(3), 286–302, doi:10.1111/j.1574-
541   6976.2012.00352.x, 2013.

542   Berman-Frank, I.: Segregation of Nitrogen Fixation and Oxygenic Photosynthesis in the Marine Cyanobacterium
543   Trichodesmium, Science, 294(5546), 1534–1537, doi:10.1126/science.1064082, 2001.

544   Berthelot, H., Bonnet, S., Camps, M., Grosso, O. and Moutin, T.: Assessment of the dinitrogen released as ammonium
545   and dissolved organic nitrogen by unicellular and filamentous marine diazotrophic cyanobacteria grown in culture,
546   Front. Mar. Sci., 2, doi:10.3389/fmars.2015.00080, 2015.

547   Berthelot, H., Bonnet, S., Grosso, O., Cornet, V. and Barani, A.: Transfer of diazotroph-derived nitrogen towards non-
548   diazotrophic planktonic communities: a comparative study between Trichodesmium erythraeum, Crocosphaera watsonii
549   and Cyanothece sp., Biogeosciences, 13(13), 4005–4021, doi:10.5194/bg-13-4005-2016, 2016.

550   Berthelot, H., Benavides, M., Moisander, P. H., Grosso, O. and Bonnet, S.: High-nitrogen fixation rates in the
551   particulate and dissolved pools in the Western Tropical Pacific (Solomon and Bismarck Seas): N 2 Fixation in the
552   Western Pacific, Geophys. Res. Lett., 44(16), 8414–8423, doi:10.1002/2017GL073856, 2017.

553   Bissett, W. P., Walsh, J. J., Dieterle, D. A. and Carder, K. L.: Carbon cycling in the upper waters of the Sargasso Sea: I.
554   Numerical simulation of differential carbon and nitrogen fluxes, Deep Sea Res. Part Oceanogr. Res. Pap., 46(2), 205–
555   269, doi:10.1016/S0967-0637(98)00062-4, 1999.

556   Bombar, D., Paerl, R. W. and Riemann, L.: Marine Non-Cyanobacterial Diazotrophs: Moving beyond Molecular
557   Detection, Trends Microbiol., 24(11), 916–927, doi:10.1016/j.tim.2016.07.002, 2016.

558   Bonnet, S., Biegala, I. C., Dutrieux, P., Slemons, L. O. and Capone, D. G.: Nitrogen fixation in the western equatorial
559   Pacific: Rates, diazotrophic cyanobacterial size class distribution, and biogeochemical significance: N 2 fixation in the
560   equatorial pacific, Glob. Biogeochem. Cycles, 23(3), n/a-n/a, doi:10.1029/2008GB003439, 2009.

561   Bonnet, S., Rodier, M., Turk-Kubo, K. A., Germineaud, C., Menkes, C., Ganachaud, A., Cravatte, S., Raimbault, P.,
562   Campbell, E., Quéroué, F., Sarthou, G., Desnues, A., Maes, C. and Eldin, G.: Contrasted geographical distribution of N
563   2 fixation rates and nif H phylotypes in the Coral and Solomon Seas (southwestern Pacific) during austral winter
564   conditions: N 2 fixation and diversity in the pacific, Glob. Biogeochem. Cycles, 29(11), 1874–1892,
565   doi:10.1002/2015GB005117, 2015b.

566   Bonnet, S., Berthelot, H., Turk-Kubo, K., Cornet-Barthaux, V., Fawcett, S., Berman-Frank, I., Barani, A., Grégori, G.,
567   Dekaezemacker, J., Benavides, M. and Capone, D. G.: Diazotroph derived nitrogen supports diatom growth in the South
568   West Pacific: A quantitative study using nanoSIMS: Transfer of diazotrophic N into plankton, Limnol. Oceanogr., 61(5),
569   1549–1562, doi:10.1002/lno.10300, 2016a.

570   Bonnet, S., Berthelot, H., Turk-Kubo, K., Fawcett, S., Rahav, E., L'Helguen, S. and Berman-Frank, I.: Dynamics
571   of N2 fixation and fate of diazotroph-derived nitrogen in a low-nutrient, low-chlorophyll ecosystem: results from the
572   VAHINE mesocosm experiment (New Caledonia), Biogeosciences, 13(9), 2653–2673, doi:10.5194/bg-13-2653-2016,
573   2016b.

574   Bonnet, S., Caffin, M., Berthelot, H. and Moutin, T.: Hot spot of N2 fixation in the western tropical South Pacific pleads
575   for a spatial decoupling between N2 fixation and denitrification, Proc. Natl. Acad. Sci., 114(14), E2800–E2801, 2017.

576   Böttjer, D., Dore, J. E., Karl, D. M., Letelier, R. M., Mahaffey, C., Wilson, S. T., Zehr, J. and Church, M. J.: Temporal
577   variability of nitrogen fixation and particulate nitrogen export at Station ALOHA: Temporal variability of nitrogen
578   fixation and particulate nitrogen, Limnol. Oceanogr., 62(1), 200–216, doi:10.1002/lno.10386, 2017.

579   Breitbarth, E., Wohlers, J., Kläs, J., LaRoche, J. and Peeken, I.: Nitrogen fixation and growth rates of Trichodesmium
580   IMS-101 as a function of light intensity, Mar. Ecol. Prog. Ser., 359, 25–36, doi:10.3354/meps07241, 2008.

581   Capone, D. G.: Trichodesmium, a Globally Significant Marine Cyanobacterium, Science, 276(5316), 1221–1229,

582   doi:10.1126/science.276.5316.1221, 1997.

583   Carpenter, E. J.: Nitrogen Fixation by a Blue-Green Epiphyte on Pelagic Sargassum, Science, 178(4066), 1207–1209,

584   doi:10.1126/science.178.4066.1207, 1972.

585   Church, M. J., Jenkins, B. D., Karl, D. M. and Zehr, J. P.: Vertical distributions of nitrogen-fixing phylotypes at Stn

586   ALOHA in the oligotrophic North Pacific Ocean, Aquat. Microb. Ecol., 38(1), 3–14, 2005.

587   Codispoti, L. A., Brandes, J. A., Christensen, J. P., Devol, A. H., Naqvi, S. W. A., Paerl, H. W. and Yoshinari, T.: The

588   oceanic fixed nitrogen and nitrous oxide budgets: Moving targets as we enter the anthropocene?, Sci. Mar., 65(S2), 85–

589   105, doi:10.3989/scimar.2001.65s285, 2001.

590   Couvelard, X., Marchesiello, P., Gourdeau, L. and Lefèvre, J.: Barotropic Zonal Jets Induced by Islands in the

591   Southwest Pacific, J. Phys. Oceanogr., 38(10), 2185–2204, doi:10.1175/2008JPO3903.1, 2008.

592   Cravatte, S., Madec, G., Izumo, T., Menkes, C. and Bozec, A.: Progress in the 3-D circulation of the eastern equatorial

593   Pacific in a climate ocean model, Ocean Model., 17(1), 28–48, doi:10.1016/j.ocemod.2006.11.003, 2007.

594   Delmont, T. O., Quince, C., Shaiber, A., Esen, O. C., Lee, S. T. M., Lucker, S. and Eren, A. M.: Nitrogen-Fixing

595   Populations Of Planctomycetes And Proteobacteria Are Abundant In The Surface Ocean, , doi:10.1101/129791, 2017.

596   Deutsch, C., Gruber, N., Key, R. M., Sarmiento, J. L. and Ganachaud, A.: Denitrification and N 2 fixation in the Pacific

597   Ocean, Glob. Biogeochem. Cycles, 15(2), 483–506, doi:10.1029/2000GB001291, 2001.

598   Deutsch, C., Sarmiento, J. L., Sigman, D. M., Gruber, N. and Dunne, J. P.: Spatial coupling of nitrogen inputs and losses

599   in the ocean, Nature, 445(7124), 163–167, doi:10.1038/nature05392, 2007.

600   Droop, M. R.: 25 Years of Algal Growth Kinetics A Personal View, Bot. Mar., 26(3), doi:10.1515/botm.1983.26.3.99,

601   1983.

602   Dupouy, C., Neveux, J., Subramaniam, A., Mulholland, M. R., Montoya, J. P., Campbell, L., Carpenter, E. J. and

603   Capone, D. G.: Satellite captures trichodesmium blooms in the southwestern tropical Pacific, Eos Trans. Am. Geophys.

604   Union, 81(2), 13, doi:10.1029/00EO00008, 2000.

605   Dupouy, C., Benielli-Gary, D., Neveux, J., Dandonneau, Y. and Westberry, T. K.: An algorithm for detecting

606   Trichodesmium surface blooms in the South Western Tropical Pacific, Biogeosciences, 8, 3631–3647, 2011.

607   Dutkiewicz, S., Ward, B. A., Monteiro, F. and Follows, M. J.: Interconnection of nitrogen fixers and iron in the Pacific

608   Ocean: Theory and numerical simulations: marine nitrogen fixers and iron, Glob. Biogeochem. Cycles, 26(1), n/a-n/a,

609   doi:10.1029/2011GB004039, 2012.

610   Falcón, L. I., Pluvinage, S. and Carpenter, E. J.: Growth kinetics of marine unicellular N₂-fixing cyanobacterial isolates

611   in continuous culture in relation to phosphorus and temperature, Mar. Ecol. Prog. Ser., 285, 3–9, 2005.

612   Fennel, K., Spitz, Y. H., Letelier, R. M., Abbott, M. R. and Karl, D. M.: A deterministic model for N 2 fixation at stn.

613   ALOHA in the subtropical North Pacific Ocean, Deep Sea Res. Part II Top. Stud. Oceanogr., 49(1), 149–174, 2001.

614   Gallon, J. R.: Reconciling the incompatible: N2 fixation And O2, New Phytol., 122(4), 571–609, doi:10.1111/j.1469-

615   8137.1992.tb00087.x, 1992.

616   Galloway, J. N., Dentener, F. J., Capone, D. G., Boyer, E. W., Howarth, R. W., Seitzinger, S. P., Asner, G. P., Cleveland,

617   C. C., Green, P. A., Holland, E. A., Karl, D. M., Michaels, A. F., Porter, J. H., Townsend, A. R. and Vörösmarty, C. J.:

618   Nitrogen Cycles: Past, Present, and Future, Biogeochemistry, 70(2), 153–226, doi:10.1007/s10533-004-0370-0, 2004.

619   Garcia, N., Raimbault, P. and Sandroni, V.: Seasonal nitrogen fixation and primary production in the Southwest Pacific:

620   nanoplankton diazotrophy and transfer of nitrogen to picoplankton organisms, Mar. Ecol. Prog. Ser., 343, 25–33,

621   doi:10.3354/meps06882, 2007.

622 Goebel, N. L., Edwards, C. A., Carter, B. J., Achilles, K. M. and Zehr, J. P.: Growth and carbon content of three
623 different-sized diazotrophic cyanobacteria observed in the subtropical north pacific, J. Phycol., 44(5), 1212–1220,
624 doi:10.1111/j.1529-8817.2008.00581.x, 2008.

625 Großkopf, T., Mohr, W., Baustian, T., Schunck, H., Gill, D., Kuypers, M. M. M., Lavik, G., Schmitz, R. A., Wallace, D.
626 W. R. and LaRoche, J.: Doubling of marine dinitrogen-fixation rates based on direct measurements, Nature, 488(7411),
627 361–364, doi:10.1038/nature11338, 2012.

628 Gruber, N.: Oceanography: A bigger nitrogen fix, Nature, 436(7052), 786–787, 2005.

629 Gruber, N.: The Marine Nitrogen Cycle: Overview and challenges, in Nitrogen in the Marine Environment, pp. 1–50,
630 Elsevier., 2008.

631 Halm, H., Lam, P., Ferdelman, T. G., Lavik, G., Dittmar, T., LaRoche, J., D'Hondt, S. and Kuypers, M. M.:
632 Heterotrophic organisms dominate nitrogen fixation in the South Pacific Gyre, ISME J., 6(6), 1238–1249,
633 doi:10.1038/ismej.2011.182, 2012.

634 Hood, R. R., Bates, N. R., Capone, D. G. and Olson, D. B.: Modeling the effect of nitrogen fixation on carbon and
635 nitrogen fluxes at BATS, Deep Sea Res. Part II Top. Stud. Oceanogr., 48(8–9), 1609–1648, doi:10.1016/S0967-
636 0645(00)00160-0, 2001.

637 Johnson, K. S., Chavez, F. P. and Friederich, G. E.: Continental-shelf sediment as a primary source of iron for coastal
638 phytoplankton, Nature, 398(6729), 697–700, doi:10.1038/19511, 1999.

639 Jullien, S., Menkes, C. E., Marchesiello, P., Jourdain, N. C., Lengaigne, M., Koch-Larrouy, A., Lefèvre, J., Vincent, E.
640 M. and Faure, V.: Impact of Tropical Cyclones on the Heat Budget of the South Pacific Ocean, J. Phys. Oceanogr.,
641 42(11), 1882–1906, doi:10.1175/JPO-D-11-0133.1, 2012.

642 Jullien, S., Marchesiello, P., Menkes, C. E., Lef?vre, J., Jourdain, N. C., Samson, G. and Lengaigne, M.: Ocean
643 feedback to tropical cyclones: climatology and processes, Clim. Dyn., 43(9–10), 2831–2854, doi:10.1007/s00382-014-
644 2096-6, 2014.

645 Karl, D., Letelier, R., Tupas, L., Dore, J., Christian, J. and Hebel, D.: The role of nitrogen fixation in biogeochemical
646 cycling in the subtropical North Pacific Ocean, Nature, 388(6642), 533–538, 1997.

647 Keith Moore, J., Doney, S. C., Lindsay, K., Mahowald, N. and Michaels, A. F.: Nitrogen fixation amplifies the ocean
648 biogeochemical response to decadal timescale variations in mineral dust deposition, Tellus B Chem. Phys. Meteorol.,
649 58(5), 560–572, doi:10.1111/j.1600-0889.2006.00209.x, 2006.

650 Krishnamurthy, A., Moore, J. K., Mahowald, N., Luo, C., Doney, S. C., Lindsay, K. and Zender, C. S.: Impacts of
651 increasing anthropogenic soluble iron and nitrogen deposition on ocean biogeochemistry: atmospheric Fe and N and
652 ocean biogoechemistry, Glob. Biogeochem. Cycles, 23(3), n/a-n/a, doi:10.1029/2008GB003440, 2009.

653 Kromkamp, J. and Walsby, A. E.: Buoyancy Regulation and Vertical Migration of Trichodesmium: a Computer-Model
654 Prediction, in Marine Pelagic Cyanobacteria: Trichodesmium and other Diazotrophs, edited by E. J. Carpenter, D. G.
655 Capone, and J. G. Rueter, pp. 239–248, Springer Netherlands, Dordrecht., 1992.

656 Küpper, H., etlk, I., Seibert, S., Pril, O., etlikova, E., Strittmatter, M., Levitan, O., Lohscheider, J., Adamska, I. and
657 Berman-Frank, I.: Iron limitation in the marine cyanobacterium Trichodesmium reveals new insights into regulation of
658 photosynthesis and nitrogen fixation, New Phytol., 179(3), 784–798, doi:10.1111/j.1469-8137.2008.02497.x, 2008.

659 Kustka, A. B., Sanudo-Wilhelmy, S. A., Carpenter, E. J., Capone, D., Burns, J. and Sunda, W. G.: Iron requirements for
660 dinitrogen-and ammonium-supported growth in cultures of Trichodesmium (IMS 101): Comparison with nitrogen
661 fixation rates and iron: carbon ratios of field populations, Limnol. Oceanogr., 48(5), 1869–1884, 2003.

662 Large, W. G., McWilliams, J. C. and Doney, S. C.: Oceanic vertical mixing: A review and a model with a nonlocal

663 boundary layer parameterization, Rev. Geophys., 32(4), 363, doi:10.1029/94RG01872, 1994.

664 LaRoche, J. and Breitbarth, E.: Importance of the diazotrophs as a source of new nitrogen in the ocean, J. Sea Res.,

665 53(1–2), 67–91, doi:10.1016/j.seares.2004.05.005, 2005.

666 Letelier, R. and Karl, D.: Trichodesmium spp. physiology and nutrient fluxes in the North Pacific subtropical gyre,

667 Aquat. Microb. Ecol., 15, 265–276, doi:10.3354/ame015265, 1998.

668 Luo, Y.-W., Doney, S. C., Anderson, L. A., Benavides, M., Berman-Frank, I., Bode, A., Bonnet, S., Boström, K. H.,

669 Böttjer, D., Capone, D. G., Carpenter, E. J., Chen, Y. L., Church, M. J., Dore, J. E., Falcón, L. I., Fernández, A., Foster,

670 R. A., Furuya, K., Gómez, F., Gundersen, K., Hynes, A. M., Karl, D. M., Kitajima, S., Langlois, R. J., LaRoche, J.,

671 Letelier, R. M., Marañón, E., McGillicuddy, D. J., Moisander, P. H., Moore, C. M., Mouriño-Carballido, B.,

672 Mulholland, M. R., Needoba, J. A., Orcutt, K. M., Poulton, A. J., Rahav, E., Raimbault, P., Rees, A. P., Riemann, L.,

673 Shiozaki, T., Subramaniam, A., Tyrrell, T., Turk-Kubo, K. A., Varela, M., Villareal, T. A., Webb, E. A., White, A. E.,

674 Wu, J. and Zehr, J. P.: Database of diazotrophs in global ocean: abundance, biomass and nitrogen fixation rates, Earth

675 Syst. Sci. Data, 4(1), 47–73, doi:10.5194/essd-4-47-2012, 2012.

676 Luo, Y.-W., Lima, I. D., Karl, D. M., Deutsch, C. A. and Doney, S. C.: Data-based assessment of environmental controls

677 on global marine nitrogen fixation, Biogeosciences, 11(3), 691–708, doi:10.5194/bg-11-691-2014, 2014.

678 Marchesiello, P., McWilliams, J. C. and Shchepetkin, A.: Open boundary conditions for long-term integration of

679 regional oceanic models, Ocean Model., 3(1–2), 1–20, doi:10.1016/S1463-5003(00)00013-5, 2001.

680 Marchesiello, P., Lefèvre, J., Vega, A., Couvelard, X. and Menkes, C.: Coastal upwelling, circulation and heat balance

681 around New Caledonia's barrier reef, Mar. Pollut. Bull., 61(7–12), 432–448, doi:10.1016/j.marpolbul.2010.06.043,

682 2010.

683 Mills, M. M., Ridame, C., Davey, M., La Roche, J. and Geider, R. J.: Iron and phosphorus co-limit nitrogen fixation in

684 the eastern tropical North Atlantic, Nature, 429(6989), 292–294, 2004.

685 Mohr, W., Großkopf, T., Wallace, D. W. R. and LaRoche, J.: Methodological Underestimation of Oceanic Nitrogen

686 Fixation Rates, edited by Z. Finkel, PLoS ONE, 5(9), e12583, doi:10.1371/journal.pone.0012583, 2010.

687 Moisander, P. H., Beinart, R. A., Voss, M. and Zehr, J. P.: Diversity and abundance of diazotrophic microorganisms in

688 the South China Sea during intermonsoon, ISME J., 2(9), 954–967, 2008.

689 Moisander, P. H., Beinart, R. A., Hewson, I., White, A. E., Johnson, K. S., Carlson, C. A., Montoya, J. P. and Zehr, J. P.:

690 Unicellular cyanobacterial distributions broaden the oceanic N2 fixation domain, Science, 327(5972), 1512–1514, 2010.

691 Moisander, P. H., Benavides, M., Bonnet, S., Berman-Frank, I., White, A. E. and Riemann, L.: Chasing after Non-

692 cyanobacterial Nitrogen Fixation in Marine Pelagic Environments, Front. Microbiol., 8, doi:10.3389/fmicb.2017.01736,

693 2017.

694 Monod, J.: Recherches sur la croissance des cultures bactériennes., Hermann & cie, Paris., 1942.

695 Monteiro, F. M., Dutkiewicz, S. and Follows, M. J.: Biogeographical controls on the marine nitrogen fixers: controls on

696 marine nitrogen fixers, Glob. Biogeochem. Cycles, 25(2), n/a-n/a, doi:10.1029/2010GB003902, 2011.

697 Montoya, J. P., Holl, C. M., Zehr, J. P., Hansen, A., Villareal, T. A. and Capone, D. G.: High rates of N2 fixation by

698 unicellular diazotrophs in the oligotrophic Pacific Ocean, Nature, 430(7003), 1027–1032, doi:10.1038/nature02824,

699 2004.

700 Moore, C. M., Mills, M. M., Arrigo, K. R., Berman-Frank, I., Bopp, L., Boyd, P. W., Galbraith, E. D., Geider, R. J.,

701 Guieu, C., Jaccard, S. L., Jickells, T. D., La Roche, J., Lenton, T. M., Mahowald, N. M., Marañón, E., Marinov, I.,

702 Moore, J. K., Nakatsuka, T., Oschlies, A., Saito, M. A., Thingstad, T. F., Tsuda, A. and Ulloa, O.: Processes and patterns

703 of oceanic nutrient limitation, Nat. Geosci., 6(9), 701–710, doi:10.1038/ngeo1765, 2013.

704 Moore, J. K., Doney, S. C., Kleypas, J. A., Glover, D. M. and Fung, I. Y.: An intermediate complexity marine ecosystem

705 model for the global domain, Deep Sea Res. Part II Top. Stud. Oceanogr., 49(1), 403–462, 2001.

706 Moore, J. K., Doney, S. C. and Lindsay, K.: Upper ocean ecosystem dynamics and iron cycling in a global three-

707 dimensional model: global ecosystem-biogeochemical model, Glob. Biogeochem. Cycles, 18(4), n/a-n/a,

708 doi:10.1029/2004GB002220, 2004.

709 Moutin, T., Van Den Broeck, N., Beker, B., Dupouy, C., Rimmelin, P. and Le Bouteiller, A.: Phosphate availability

710 controls Trichodesmium spp. biomass in the SW Pacific Ocean, Mar. Ecol. Prog. Ser., 297(1), 15–21, 2005.

711 Moutin, T., Karl, D. M., Duhamel, S., Rimmelin, P., Raimbault, P., Van Mooy, B. A. S. and Claustre, H.: Phosphate

712 availability and the ultimate control of new nitrogen input by nitrogen fixation in the tropical Pacific Ocean,

713 Biogeosciences, 5(1), 95–109, doi:10.5194/bg-5-95-2008, 2008.

714 Mulholland, M. R. and Capone, D. G.: The nitrogen physiology of the marine N2-fixing cyanobacteria Trichodesmium

715 spp., Trends Plant Sci., 5(4), 148–153, doi:10.1016/S1360-1385(00)01576-4, 2000.

716 Mulholland, M. R., Ohki, K. and Capone, D. G.: Nutrient controls on nitrogen uptake and metabolism by natural

717 populations and cultures of Trichodesmium (cyanobacteria), J. Phycol., 37(6), 1001–1009, doi:10.1046/j.1529-

718 8817.2001.00080.x, 2001.

719 Neveux, J., Tenírio, M. M. B., Dupouy, Cé. and Villareal, T. A.: Spectral diversity of phycoerythrins and diazotroph

720 abundance in tropical waters, Limnol. Oceanogr., 51(4), 1689–1698, doi:10.4319/lo.2006.51.4.1689, 2006.

721 Ohki, K., Zehr, J. P. and Fujita, Y.: Regulation of nitrogenase activity in relation to the light-dark regime in the

722 filamentous non-heterocystous cyanobacterium Trichodesmium sp. NIBB 1067, Microbiology, 138(12), 2679–2685,

723 1992.

724 Paerl, H. W., Priscu, J. C. and Brawner, D. L.: Immunochemical localization of nitrogenase in marine Trichodesmium

725 aggregates: Relationship to N2 fixation potential, Appl. Environ. Microbiol., 55(11), 2965–2975, 1989.

726 Penven, P., Debreu, L., Marchesiello, P. and McWilliams, J. C.: Evaluation and application of the ROMS 1-way

727 embedding procedure to the central california upwelling system, Ocean Model., 12(1–2), 157–187,

728 doi:10.1016/j.ocemod.2005.05.002, 2006.

729 Postgate, J. R.: Biology nitrogen fixation: fundamentals, Philos. Trans. R. Soc. Lond. B Biol. Sci., 296(1082), 375–385,

730 1982.

731 Radic, A., Lacan, F. and Murray, J. W.: Iron isotopes in the seawater of the equatorial Pacific Ocean: New constraints

732 for the oceanic iron cycle, Earth Planet. Sci. Lett., 306(1–2), 1–10, doi:10.1016/j.epsl.2011.03.015, 2011.

733 Raimbault, P. and Garcia, N.: Evidence for efficient regenerated production and dinitrogen fixation in nitrogen-deficient

734 waters of the South Pacific Ocean: impact on new and export production estimates, Biogeosciences, 5(2), 323–338,

735 2008.

736 Ramamurthy, V. D. and Krishnamurthy, S.: Effects of N: P ratios on the uptake of nitrate and phosphate by laboratory

737 cultures ofTrichodesmium erythraeum (Ehr.), Proc. Plant Sci., 65(2), 43–48, 1967.

738 Raven, J. A.: The iron and molybdenum use efficiencies of plant growth with different energy, carbon and nitrogen

739 sources, New Phytol., 109(3), 279–287, doi:10.1111/j.1469-8137.1988.tb04196.x, 1988.

740 Rubin, M., Berman-Frank, I. and Shaked, Y.: Dust- and mineral-iron utilization by the marine dinitrogen-fixer

741 Trichodesmium, Nat. Geosci., 4(8), 529–534, doi:10.1038/ngeo1181, 2011.

742 Rueter, J. G.: Iron stimulation of photosynthesis and nitrogen fixation in Anabaena 7120 and Trichodesmium

743 (Cyanophyceae), J. Phycol., 24(2), 249–254, doi:10.1111/j.1529-8817.1988.tb04240.x, 1988.

744 Shchepetkin, A. F. and McWilliams, J. C.: Quasi-Monotone Advection Schemes Based on Explicit Locally Adaptive

745 Dissipation, Mon. Weather Rev., 126(6), 1541–1580, doi:10.1175/1520-0493(1998)126<1541:QMASBO>2.0.CO;2,
746 1998.

747 Shchepetkin, A. F. and McWilliams, J. C.: The regional oceanic modeling system (ROMS): a split-explicit, free-surface,
748 topography-following-coordinate oceanic model, Ocean Model., 9(4), 347–404, doi:10.1016/j.ocemod.2004.08.002,
749 2005.

750 Shiozaki, T., Kodama, T., Kitajima, S., Sato, M. and Furuya, K.: Advective transport of diazotrophs and importance of
751 their nitrogen fixation on new and primary production in the western Pacific warm pool, Limnol. Oceanogr., 58(1), 49–
752 60, doi:10.4319/lo.2013.58.1.0049, 2013.

753 Shiozaki, T., Kodama, T. and Furuya, K.: Large-scale impact of the island mass effect through nitrogen fixation in the
754 western South Pacific Ocean: island mass effect through N2 fixation, Geophys. Res. Lett., 41(8), 2907–2913,
755 doi:10.1002/2014GL059835, 2014.

756 Shiozaki, T., Nagata, T., Ijichi, M. and Furuya, K.: Nitrogen fixation and the diazotroph community in the temperate
757 coastal region of the northwestern North Pacific, Biogeosciences, 12(15), 4751–4764, doi:10.5194/bg-12-4751-2015,
758 2015.

759 Staal, M., Filip, Meysman and Lucas: Temperature excludes N2-fixing heterocystous cyanobacteria in the tropical
760 oceans, Nature, 425(6957), 501–504, doi:10.1038/nature02001, 2003.

761 Sunda, W. G. and Huntsman, S. A.: Interrelated influence of iron, light and cell size on marine phytoplankton growth,
762 Nature, 390(6658), 389–392, doi:10.1038/37093, 1997.

763 Tagliabue, A., Bopp, L. and Aumont, O.: Ocean biogeochemistry exhibits contrasting responses to a large scale
764 reduction in dust deposition, Biogeosciences, 5(1), 11–24, 2008.

765 Tagliabue, A., Bopp, L., Dutay, J.-C., Bowie, A. R., Chever, F., Jean-Baptiste, P., Bucciarelli, E., Lannuzel, D.,
766 Remenyi, T., Sarthou, G., Aumont, O., Gehlen, M. and Jeandel, C.: Hydrothermal contribution to the oceanic dissolved
767 iron inventory, Nat. Geosci., 3(4), 252–256, doi:10.1038/ngeo818, 2010.

768 Tagliabue, A., Mtshali, T., Aumont, O., Bowie, A. R., Klunder, M. B., Roychoudhury, A. N. and Swart, S.: A global
769 compilation of dissolved iron measurements: focus on distributions and processes in the Southern Ocean,
770 Biogeosciences, 9(6), 2333–2349, doi:10.5194/bg-9-2333-2012, 2012.

771 Toner, B. M., Fakra, S. C., Manganini, S. J., Santelli, C. M., Marcus, M. A., Moffett, J. W., Rouxel, O., German, C. R.
772 and Edwards, K. J.: Preservation of iron(II) by carbon-rich matrices in a hydrothermal plume, Nat. Geosci., 2(3), 197–
773 201, doi:10.1038/ngeo433, 2009.

774 Turk-Kubo, K. A., Karamchandani, M., Capone, D. G. and Zehr, J. P.: The paradox of marine heterotrophic nitrogen
775 fixation: abundances of heterotrophic diazotrophs do not account for nitrogen fixation rates in the Eastern Tropical
776 South Pacific: N 2 -fixing potential of heterotrophs in the ETSP, Environ. Microbiol., 16(10), 3095–3114,
777 doi:10.1111/1462-2920.12346, 2014.

778 Villareal, T. A. and Carpenter, E. J.: Diel buoyancy regulation in the marine diazotrophic cyanobacterium
779 Trichodesmium thiebautii, Limnol. Oceanogr., 35(8), 1832–1837, doi:10.4319/lo.1990.35.8.1832, 1990.

780 Villareal, T. A. and Carpenter, E. J.: Buoyancy Regulation and the Potential for Vertical Migration in the Oceanic
781 Cyanobacterium Trichodesmium, Microb. Ecol., 45(1), 1–10, doi:10.1007/s00248-002-1012-5, 2003.

782 White, A., Spitz, Y. and Letelier, R.: Modeling carbohydrate ballasting by Trichodesmium spp., Mar. Ecol. Prog. Ser.,
783 323, 35–45, doi:10.3354/meps323035, 2006.

784 Ye, Y., Völker, C., Bracher, A., Taylor, B. and Wolf-Gladrow, D. A.: Environmental controls on N2 fixation by
785 Trichodesmium in the tropical eastern North Atlantic Ocean—A model-based study, Deep Sea Res. Part Oceanogr. Res.

786   Pap., 64, 104–117, doi:10.1016/j.dsr.2012.01.004, 2012.

787   Zehr, J. P. and Bombar, D.: Marine Nitrogen Fixation: Organisms, Significance, Enigmas, and Future Directions, in

788   Biological Nitrogen Fixation, edited by F. J. de Bruijn, pp. 855–872, John Wiley & Sons, Inc, Hoboken, NJ, USA.,

789   2015.

Table 1 : Models parameters for Trichodemium and nanophytoplakton.

Parameters	Symbol	Name in code	Unity	Value
Initial slope P-I tricho	αI	pislope1	$(W.m^{-2})^{-1} d^{-1}$	0.072
Initial slope P-I nano	αI	pislope	$(W m^{-2})^{-1} d^{-1}$	2.0
Microzoo preference for tricho	pItri	xpref2t	-	0.5
Microzoo preference for nano	pIP	xpref2p	-	1.0
Mesozoo preference for tricho	pItri	xpreft	-	0.3
Mesozoo preference for nano	pIP	xprefp	-	0.3
Tricho feeding threshold for mesozoo	Tithresh	xthresh2tri	$mol\ C\ L^{-1}$	1.10^{-8}
Nanophyto feeding threshold for mesozoo	Pithresh	xthresh2phy	$mol\ C\ L^{-1}$	1.10^{-8}
Tricho feeding threshold for microzoo	Tithresh	xthreshtri	$mol\ C\ L^{-1}$	1.10^{-8}
Nanophyto feeding threshold for microzoo	Pithresh	xthreshphy	$mol\ C\ L^{-1}$	1.10^{-8}
NO3 half saturation of tricho	KTriNO3	conctno3	$mol\ N\ L^{-1}$	1.10^{-6}
NO3 half saturation of nanophyto	KPNO3	concnno3	$mol\ N\ L^{-1}$	1.10^{-6}
NH4 half saturation of tricho	KTriNH4	conctnh4	$mol\ N\ L^{-1}$	5.10^{-7}
NH4 half saturation of nanophyto	KPNH4	concnnh4	$mol\ N\ L^{-1}$	5.10^{-7}
PO4 half saturation of tricho	KTriPO4	conctpo4	$mol\ P\ L^{-1}$	5.10^{-6}
PO4 half saturation of nanophyto	KPPO4	concnpo4	$mol\ P\ L^{-1}$	5.10^{-6}
Iron half saturation for tricho	KtriFe	conctfer	$mol\ Fe\ L^{-1}$	1.10^{-9}
Iron half saturation for nanophyto	KPFe	concnfer	$mol\ Fe\ L^{-1}$	1.10^{-9}
Minimum size criteria for tricho	Imax	xsizetri	$mol\ C\ L^{-1}$	1.10^{-6}
Minimum size criteria for nanophyto	Imax	xsizephy	$mol\ C\ L^{-1}$	1.10^{-6}
Optimal Fe quota for tricho	θFe,Triopt	qtfelim	$mol\ Fe\ (mol\ C)^{-1}$	7.10^{-6}
Optimal Fe quota for nanophyto	θFe,Iopt	qnfelim	$mol\ Fe\ (mol\ C)^{-1}$	7.10^{-6}
Minimum Chl/C in tricho	θChl,Trimin	chlctm	$mg\ Chl\ (mg\ C)^{-1}$	0.033
Minimum Chl/C in nanophyto	θChl,Imin	chlcnm	$mg\ Chl\ (mg\ C)^{-1}$	0.033
Maximum Fe/C in tricho	θFe,Trimax	fectm	$mol\ Fe\ (mol\ C)^{-1}$	1.10^{-4}
Maximum Fe/C in nanophyto	θFe,Imax	fecnm	$mol\ Fe\ (mol\ C)^{-1}$	4.10^{-5}
Maximum N/C in tricho	θN,Trimax	qntlm	$mol\ N\ (mol\ C)^{-1}$	1.45
Maximum N/C in nanophyto	θN,Imax	qnnlm	$mol\ N\ (mol\ C)-1$	1.45
Maximum P/C in tricho	θP,Trimax	qptlm	$mol\ P\ (mol\ C)^{-1}$	2.44
Maximum P/C in nanophyto	θN,Imax	qpnlm	$mol\ P\ .(mol\ C)^{-1}$	2.44
Excretion ratio of tricho	rTri	excret1	d^{-1}	0.05
Excretion ratio of nanophyto	rI	excret	d^{-1}	0.05
Maintenance iron	m	zfixbasal	$mol\ Fe\ .(mol\ C)^{-1}$	$1.4.10^{-5}$
Marginal use efficiency	β	qfec	day^{-1}	$1.4.10^{-4}$

Table 2 : List and description of the different experiments.

Name configuration	N$_2$ fixation	Iron from sediment
TRI	explicit	yes
TRI_NoFeSed	explicit	no
N2_imp	implicit	yes
Wo_N2	no	yes

790 **Figures caption**

Fig. 1 : Annual mean concentrations in μmol L^{-1}: a) PO4 data from the CARS b) PO4 simulated by ROMS-PISCES model c) NO3 data from the CARS d) NO3 simulated by ROMS-PISCES model. On panels a and b the black contours show the annual mean of patterns of temperature prefenrendum from observations (a) and model (b). The red contours displays the 26°C isolign for austral winter (plain) and austral summer (dash). On panels (c) and (d) the red boxes represent the LNLC regions.

Fig. 2 : Left : Boxplots of the 0-150 averaged Iron (nmol Fe.L^{-1}) data (blue) and the equivalent for the model (red) colocalised with the observations in space. The coloured box represents the 25-75% of the distribution, the whiskers the 10-90% distribution. The line into the coloured box is the median.

Right : Iron concentrations (nmol Fe.L^{-1}) as observed (b) and as simulated by the model (c). Iron concentrations has been averaged over the top 150m of the ocean. Model values have been sampled at the same location, the same month, and the same depth as the data.

Fig. 3 : Top : Annual mean Chlorophyll concentration (in mg Chl.m^{-3}) in surface from (a) GLOBCOLOUR data (b) TRI simulation (c) TRI_imp simulation.

Bottom (d) : Annual mean Trichodesmium chlorophyll (in mg Chl.m^{-3}) in surface from TRI simulation

Fig. 4 : Nitrogen fixation rates (μmol N.m^{-2}d^{-1}) as observed (left) and as simulated by TRI simulation (right).

Top : Nitrogen fixation rates has been integrated over the top 150m of the ocean.

Bottom : Nitrogen fixation rates has been averaged over the top 30m of the ocean.

Model values have been sampled at the same location, the same month, and the same depth as the data.

Fig. 5 : a) Depth-integrated (0 to 125m) rates of nitrogen fixation (μmol N.m^{-2}d^{-1}) at ALOHA for the data (blue) and TRI simulation (red).

b) Depth-integrated (0 to 150m) rates of nitrogen fixation (μmol N.m^{-2}d^{-1}) in the south pacific (red box, Fig. 1c) for the data (blue) and TRI simulation (red). The green curve is the averaged of the seasonal cycle from TRI simulation at the data positions. Model values have been sampled at the same location, the same month, and the same depth as the data.

Fig. 6 : Relative contribution (in percentage) of *Trichodesmium* to primary production.

Fig. 7 : *Trichodesmium* biomass (mmol C.m^{-2}) for a) austral summer and b) austral winter, integrated over the top 100m of the ocean.

Fig. 8 : Seasonal cycle of limitation terms for *Trichodesmium* production in a) South Pacific and b) North Pacific. The right scale represents the total limitation.

Fig. 9 : Top : Minimum, mean and maximum in the South box (Fig 1c) for (a) iron concentration, (b) chlorophyll concentration in Trichodesmium.

Bottom : Annual mean iron concentration (shading ; in nmol Fe.L^{-1}) and current (vectors ; in m.s^{-1}) for c) TRI_NoFeSed simulation and d) TRI simulation. Annual mean Chlorophyll concentration in *Trichodesmium* (mg Chl.m^{-3}) for e) TRI_NoFeSed simulation and f) TRI simulation. The concentrations have been averaged over the top 100m of the ocean.

Fig. 10 : Percentage increase of primary production between the TRI simulation and Wo_N2 simulation (top) and N2_imp simulation (bottom); for total primary production (left) and primary production from Nanophyto. + diatoms (right).
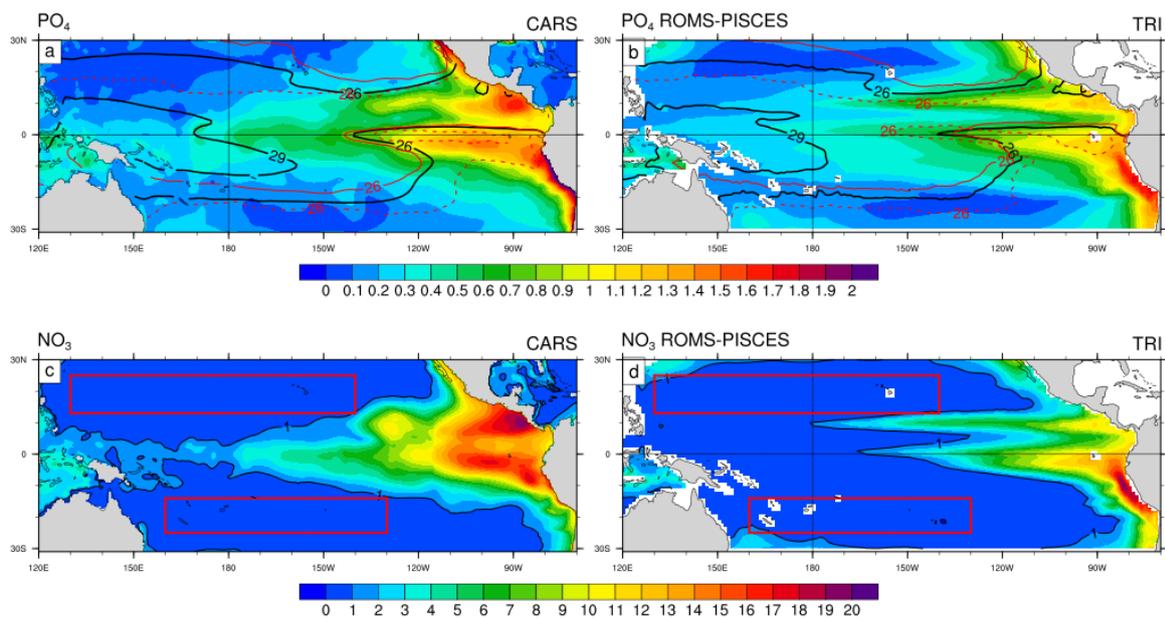
Figure 1
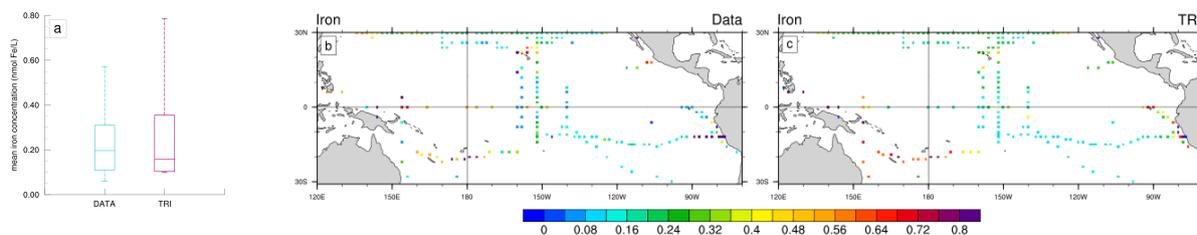
Figure 2
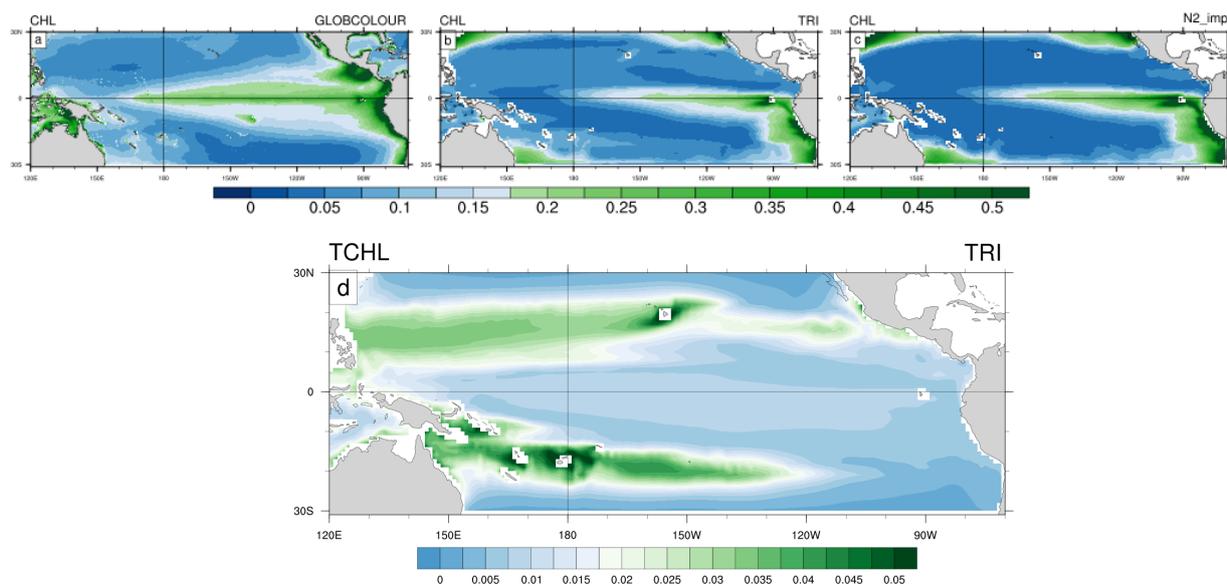
Figure 3
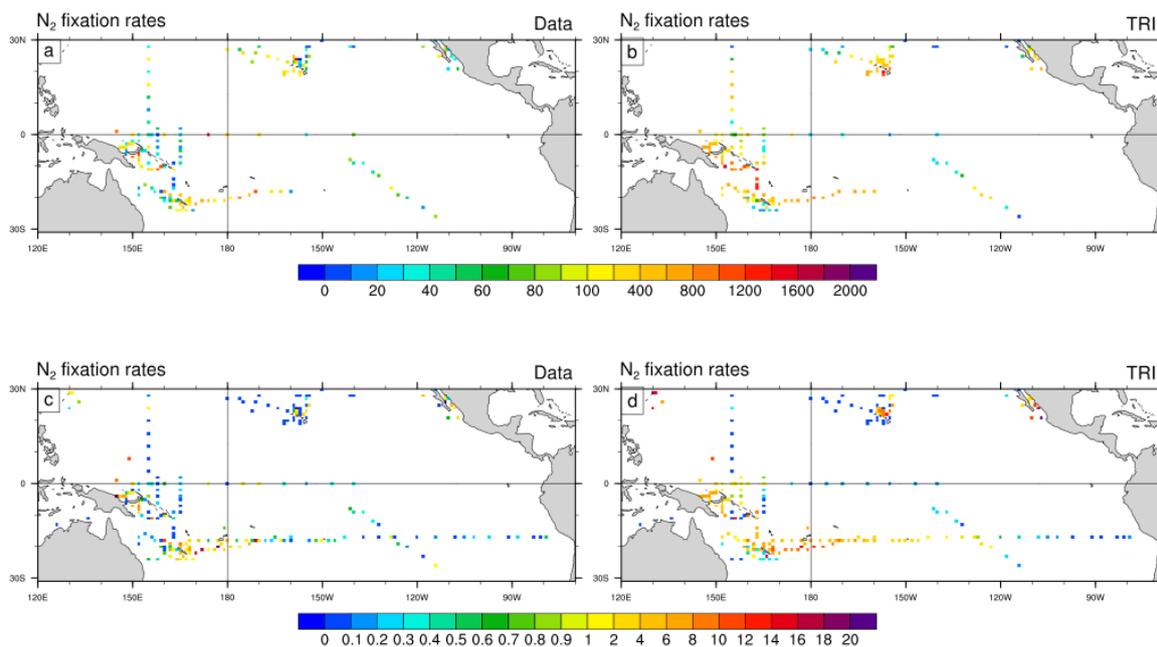
Figure 4
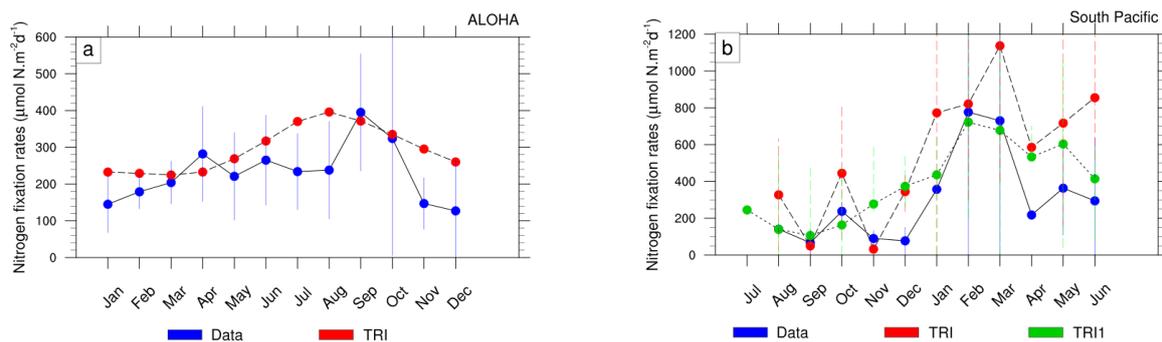
Figure 5
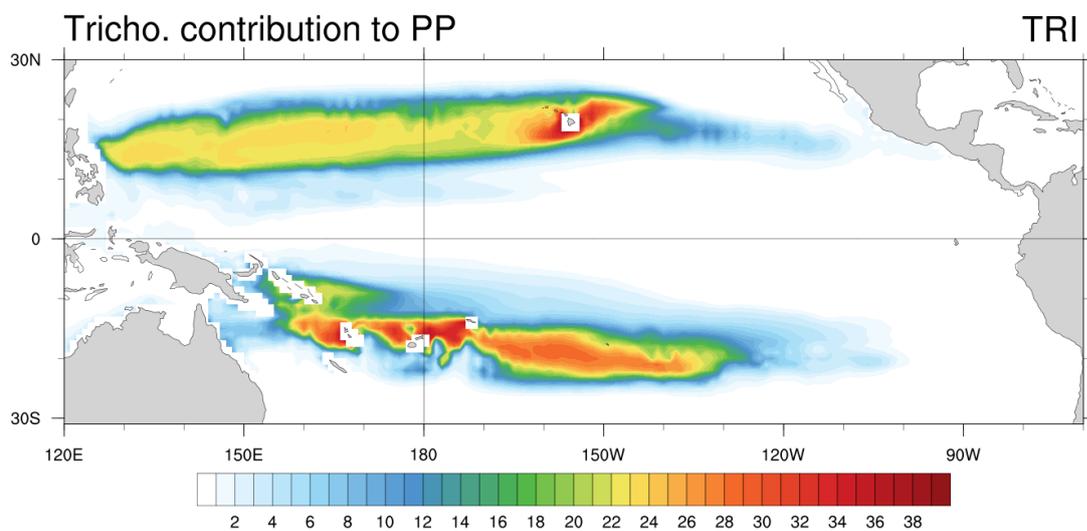
Figure 6
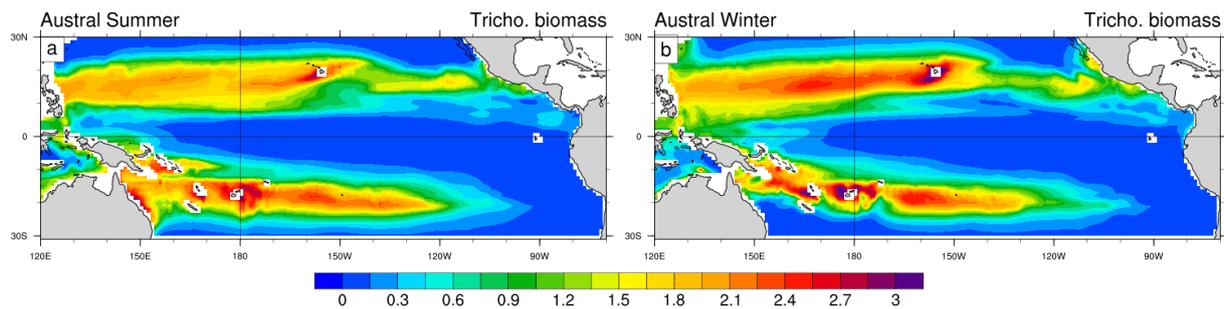
Figure 7
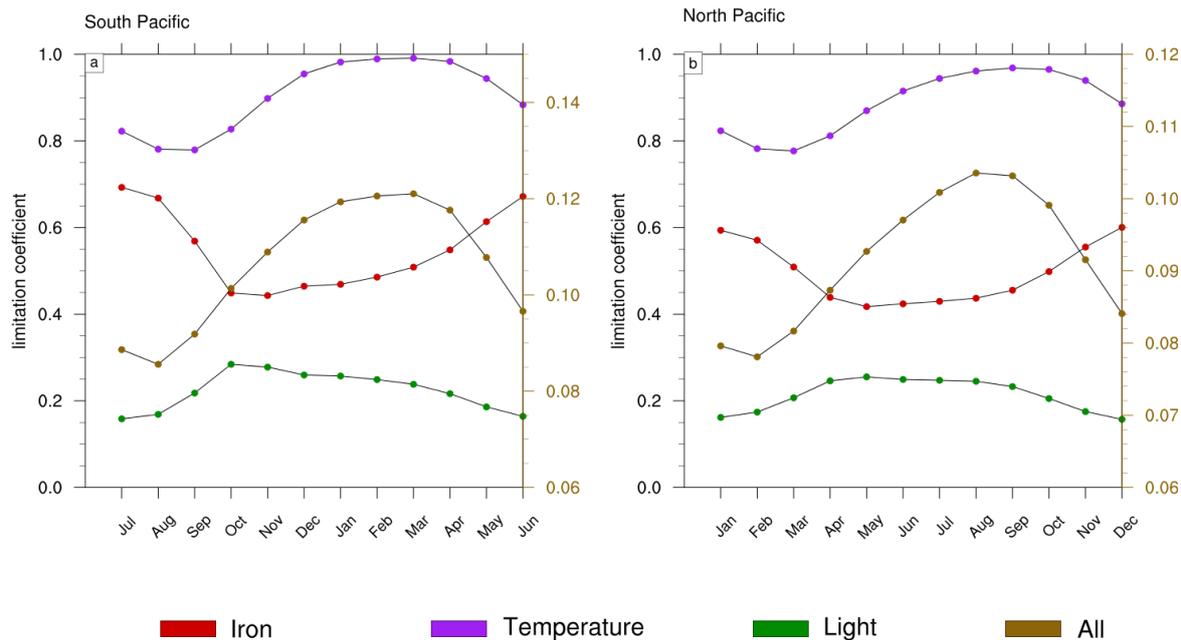
Figure 8

Figure 9

Figure 10